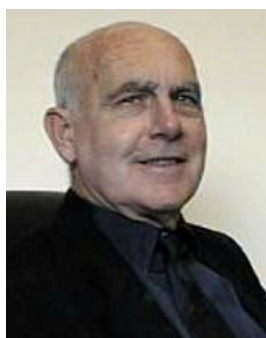


THE ESTIMATION OF SLAG PROPERTIES



Ken Mills

Department of Materials, Imperial College, London, UK

kcmills@talktalk.net

Short course presented as part of

Southern African Pyrometallurgy 2011

7 March 2011

Symbols and Units

a =thermal diffusivity (m^2s^{-1})
 C_p = Heat capacity ($\text{JK}^{-1}/\text{mol}$ or kg)
 E = Extinction coefficient (m^{-1})
 E = Activation energy (kJ mol^{-1})
 f = fraction of M^{3+} ions acting as network breaker
 $(H_T - H_{298})$ = Enthalpy (J/mol or kg)
 ΔH^{fus} = enthalpy of fusion (JK/mol or kg)
 k = thermal conductivity ($\text{Wm}^{-1}\text{K}^{-1}$)
 K = Electrical conductivity (Ωm^{-1})
 k =Thermal conductivity ($\text{W}^{-1}\text{K}^{-1}$)
 (l) = liquid phase
 M = molecular weight (g mol^{-1})
 n = refractive index
 P = property
 p = partial pressure (atm , bar)
 Q = $4-(\text{NBO}/T)$ = measure of polymerisation
 R = electrical resistivity ($=1/\kappa$) (Ωm)
 R^* = Gas Constant= 8.314 ($\text{JK}^{-1}\text{mol}^{-1}$)
 s^* = scattering coefficient (m^{-1})
 (s) = solid phase
 T = temperature (K or $^{\circ}\text{C}$)
 T_g = Glass transition temperature (K or $^{\circ}\text{C}$)
 T_{liq} = liquidus temperature (K or $^{\circ}\text{C}$)
 T_{sol} = solidus temperature (K or $^{\circ}\text{C}$)
 V = molar volume ($\text{m}^3 \text{mol}^{-1}$)
 α = linear thermal expansion coefficient (K^{-1})
 α^* = Absorption coefficient (m^{-1})
 β = volume thermal expansion coefficient (K^{-1})
 ε = emissivity
 γ =surface tension (mNm^{-1})
 γ_{ms} =slag/metal interfacial tension (mNm^{-1})

ε = emissivity
 κ =electrical conductivity ($\Omega^{-1}\text{m}^{-1}$)
 Λ = Optical basicity
 η = viscosity (Pas or dPas)
 θ = contact angle ($^{\circ}$)
 ρ = density (kgm^{-3})

Subscripts and superscripts

br = break (temperature)
 liq = liquidus
 $^{\text{m}}$ (superscript)=value at T_{liq}
 $_{\text{m}}$ (subscript)= metal
 $^{\text{m}}$ (superscript)=value at T^{liq}
 s = slag
 sol = solidus

Abbreviations

AL = aerodynamic levitation
 BF = Blast furnace
 BO = Bridging Oxygen
 BOS =Basic Oxygen Steelmaking process
 CC = Continuous casting of steel
 de-S = de-sulphurisation
 EML = Electro-magnetic levitation
 ESL = Electro-static levitation
 ESR = Electro-slag refining
 NBO = Non-bridging Oxygen
 NBO/T = non bridging O/ tetragonal O
 scl = super-cooled liquid

Contents

1. SLAGS

1.1 Slag Properties	1		
1.1.1 Reactivity of slag with container, metal and atmosphere	2	Mechanism of erosion of carbon/oxide refractories	5
Slag/container reactions	2	How to combat slag/erosion of refractories	6
Slag/metal reactions	3		
Slag/atmosphere reactions	3	1.1.2 Thermo-physical properties	7
Corrosion and erosion of refractories	3		
Mechanism of slag line erosion	4	1.1.3 Estimation of thermo-physical properties	7
		Partial Molar properties	7

2. STRUCTURE OF SLAGS

2.1 Structure of slags and glasses	7	2.4 Effect of structure on properties	11
2.2 Parameters used to represent structure	9	2.4.1 Effect of structure (NBO/T or Q) on properties	11
2.2.1 NBO/T and Q	9	Viscosity	11
2.2.2 Optical basicity	10	Thermal & electrical conductivity	12
		Thermal expansion and density	12
2.3 Structural changes in glasses and slags with temperature	10	Surface tension and emissivity	13
		Heat capacity and entropy of fusion	13

3. TYPES OF MODEL

3.1 Numerical fits	14	3.4 Thermodynamic models	16
3.2 Neural networks	14	3.5 Molecular Dynamics models	17
3.3 Models based on structure	15		

4. MODELLING PHYSICAL PROPERTIES

4.1 Liquidus and solidus temperatures	17	4.5 Viscosities	21
4.2 Heat Capacity, enthalpy	17	4.6 Electrical conductivity	23
4.3 Thermal expansion	19	4.7 Surface tension	26
4.4 Density	20	4.8 Thermal conductivity	29

5. THE MODEL

5.1 composition worksheet	35	References	42
5.2 Collected worksheet	35		
5.3 Cp and enthalpy worksheet	36	Appendix 1: Methods used to determine structure	47
5.4 Density worksheet	36	Appendix 2: Details of MLL model	49
5.5 Surface tension worksheet	37		
5.6 Viscosity Worksheet	37		
5.7 Thermal conductivity worksheet	40		
5.6 Electrical conductivity worksheet	42		

1. SLAGS

The word “slags” may not have a pleasant connotation with the man in the street but they are very important to metal production. They protect the metal and remove undesirable impurities. Usually a liquid slag layer covers the molten metal and carries out the following functions:

- (i) It seals off the metal from oxygen and prevents oxidation
- (ii) It removes undesirable elements (eg. S ,P) from the metal
- (iii) It helps to remove non-metallic inclusions (eg by flotation etc)
- (iv) It reduces the heat losses from the metal surface and prevents the “skull formation” and
- (v) in the continuous casting of steel liquid slag infiltrates continuously between the metal and mould and it provides both lubrication and control of the heat extraction.

Slags are very important to the production of clean metals. The old adage “*Look after the slag and the metal will look after itself*” is very appropriate.

Slags have a wide range of composition:

Metallurgical slags are usually based on the CaO-Al₂O₃- SiO₂ system

Non-ferrous slags are frequently based on fayalite- eg FeO.SiO₂

Coal slags/ fly ashes are basically CaO+Al₂O₃ + SiO₂ with relatively low CaO levels (<10%) and tend to be very viscous

ESR-slags are made of oxides and fluorides (in significant amounts) eg CaF₂+ CaO+ Al₂O₃

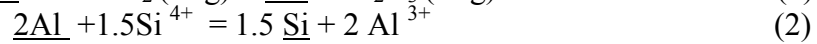
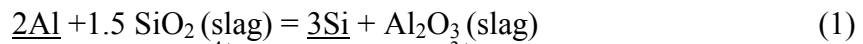
Continuous casting fluxes and welding fluxes are made up of oxides with <10% CaF₂

Slags have similarities to glasses and slugs.

Glasses- tend to have high SiO₂ contents

Enamels contain appreciable amounts of B₂O₃

Liquid slags are thought to be made up of ions. We know that ions are involved in reactions between metal and slag; eg reaction 1 can be expressed by Equation 2 (where M indicates in metal) :



These electro-chemical reactions are accompanied by changes in properties. Mass transfer (in Equation 1) across the metal/slag interface is accompanied (Figure 1)by (i) decrease in interfacial tension (which causes local turbulence and easy transfer across the interface) and (ii)a gradual decrease in the potential difference between metal and slag. The local interfacial turbulence is also a result of the changes in electrical potential which result in local changes in surface tension which, in turn, induce Marangoni flows (arising from surface tension gradients).

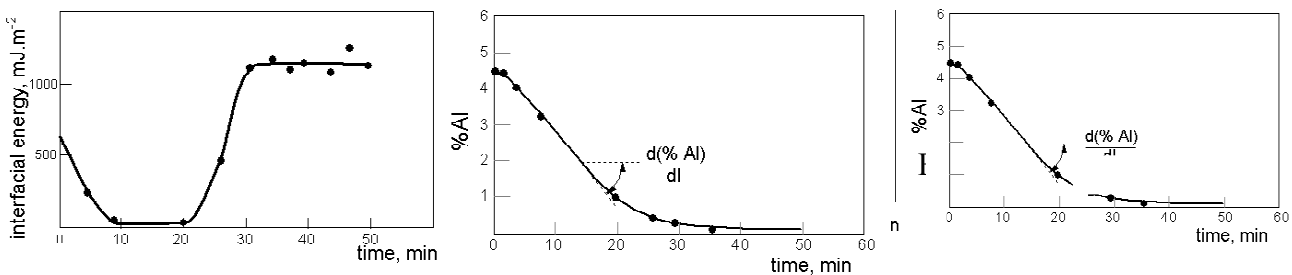


Figure 1 Figure Changes in (i) interfacial tension (ii)Mass transfer (iii) Electrical potential for reaction 1 [1].

1.1 Slag properties

Slag properties are important since they:

- (i) have a decisive effect on both process control and on the quality of the product and

- (ii) good quality property data are needed to develop reliable mathematical models of the process and to optimise the efficiency of the process and quality control.

An example of process control is that the slag compositions should have a high S-capacity to maximise transfer of S from the metal to slag; this is usually achieved by using a liquid, high-basicity flux. If de-sulphurisation (d-S) is below requirement more CaO is added to increase basicity but it could also increase the liquidus temperature (T_{liq}) of the slag and thereby reduce the amount of liquid slag formed, which, in turn, results in less de-sulphurisation.

An example of the effect on product quality occurs in continuous casting (CC). Longitudinal cracks occur on the surface of the steel and have to be scarfed off, thereby reducing yield and increasing expenditure and energy. It is known that flux viscosity (η) and break temperature (T_{br}) of mould fluxes used in CC must be optimised to eradicate longitudinal cracking.

There are several types of mathematical model namely (i) *thermodynamic models* (to establish the viability of the process and the optimum conditions) (ii) *kinetic models* (to establish that the productivity rate) (iii) *heat and fluid flow models* (to improve process design and control) and (iv) models of *environmental and financial impact* of the process. Reliable property values are principally needed as input data for heat and fluid flow models.

1.1.1 Reactivity of slag with container, metal and atmosphere

The unofficial First law of High Temperatures states:

”At high temperatures everything reacts with everything else”

and the Second Law states

“They react bloody quickly and it gets exponentially- worse as the temperature increases “.

Slags react with the container and any other contact materials (eg. bobs) with the metal and with the atmosphere. Their reactivity varies between the viscously aggressive (eg coal slags and ashes) to benign (glasses) and is very dependent upon the slag composition.

Some slags are basically unstable at high temperatures since two or more components in the slag will react and the composition will change continuously eg ESR slags where fluorides and oxides react eg.



and the slag composition shows a steady increase in CaO concentration and a decrease in Al_2O_3 .

Slag/container reactions

Some slags are so aggressive and reactive towards the refractory walls that a process has had to be abandoned because no suitable refractory could be identified. (Slag /refractory erosion is discussed in more detail below).

A major problem in performing measurements on slags involves the selection of a crucible material which is inert to the slag. The general rule in selecting crucibles is *“Use a metal to contain an oxide melt and use a refractory oxide to contain liquid metals”*. The most commonly-used materials are either (i) Pt metals and alloys (eg. Pt, Ir) or (ii) refractory metals (Mo, Ta, W). Pt-alloys are not suitable for reducing conditions and Mo etc are not suitable for oxidising conditions. FeO- containing slags are notoriously aggressive since FeO is easily reduced by the container (see Figure 2); it is customary to use Fe crucibles but this limits the temperature range to $<1400^\circ\text{C}$. Graphite is also widely used but (i) reacts with slag oxides (eg. $\text{FeO}_{\text{slag}} + \text{C} = \text{CO}(\text{g}) + \text{Fe}$) and (ii) is non-wetting which affects viscosity measurements) Container-less methods have been used to avoid slag/container reactions (eg levitation (EML, ESL, AL and micro-gravity conditions) [2]

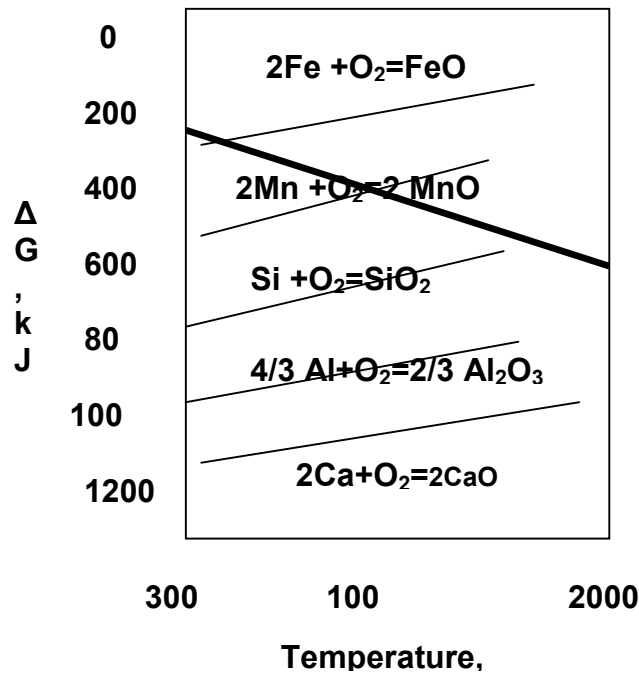


Figure 2: Schematic Ellingham diagram; (i) Any element lower in the diagram will capture O from an element above (Al will take O from FeO) (ii) Oxides reduced by C when $T > T_{\text{crossover}}$ of $2\text{C} + \text{O}_2 = 2\text{CO}$ (Bold line) with other curves

Slag/metal reactions

Slag/metal reactions are very important in the production of clean metals (eg. de-S and de-P) but they can sometimes produce unwanted reactions (eg. Eqn 1 i.e. $\text{SiO}_2_{\text{slag}} + \text{Al} = \text{Si} + \text{Al}_2\text{O}_3_{\text{slag}}$) in continuous casting (CC). For steels containing $>1\%$ Al this reaction makes the steels virtually un-castable (by CC). Slag/metal reactions involve ions (Eqn 1) and involve charge exchange resulting in the changes shown in Figure 1.

Slag/atmosphere reactions

The slag is used in many processes to shield the metal from oxidation; oxygen can have a significant effect on transition-metal, multi-valent oxides (eg. $\text{Fe}^{2+}/\text{Fe}^{3+}$, $\text{Cr}^{2+}/\text{Cr}^{3+}$, Ti-Nb-oxides). In the case of $\text{Fe}^{2+}/\text{Fe}^{3+}$, the Fe_2O_3 concentration has a significant effect on the properties (eg. viscosity, electrical resistivity). Thus it is important that the partial pressure of oxygen, p_{O_2} , in an experiment be selected to reflect the conditions of the industrial process being studied.

Nitrogen tends to be inert to most slags but those containing Ti and Nb will react with N_2 to form TiN and NbN inclusions, which can have significant effects on the process.

Reactions of slags with moisture can have important effects. In oxide slags with the H_2O being both chemically-bonded to the slag and adsorbed on the slag; this can affect the performance of the slags. However, the effects of moisture are more severe when dealing with slags containing fluorides, (or chlorides) such as ESR fluxes, CC fluxes and Al fluxes because of the reaction :



The $\text{HF}(\text{g})$ emitted can cause plant corrosion and pose a threat to health of the plant personnel.

Corrosion and Erosion of refractories

Corrosion is the chemical attack of refractories

Erosion involves both the chemical attack (erosion) and the mechanical abrasion of the refractory.

Refractories (eg Al_2O_3 , CaO , MgO and ZrO_2) used for furnace linings are usually oxides with great chemical stability (see Ellingham diagram, Figure 2) and have high melting points. These properties arise from the great chemical affinity of Al, Ca, Mg and Zr for oxygen (the bond strength Al-O etc. is very high) – these elements lie at the bottom of the Ellingham diagram and it is very difficult for metals to break the Al-O bond and form a metal-oxide bond. However, most slags will dissolve a certain amount of the refractory oxide eg. CC fluxes dissolve up to 40% Al_2O_3 , up to 10% TiO_2 and only 2% ZrO_2 and 0.5% TiN .



Figure 3: Schematic drawing of BOS process and the turbulence generated which causes refractory erosion

Erosion frequently arises from turbulent flows generated in the converter eg. the BOS process (Figure 3) or from mechanical erosion eg the feeding of scrap to the converter. Enhanced erosion tends to occur in furnace linings at the metal / slag and slag/ atmosphere interfaces; this is known as “slag line erosion”.

Mechanism of slag line erosion

The refractories used in industrial furnaces frequently exhibit a n area of wear (deep groove) in the region between the slag/metal and slag/gas interfaces. Figure 4 shows the case of slag line attack at the slag/atmosphere interface for a SiO_2 refractory; the same mechanism is thought to apply to other refractories. When the slag first comes in contact with the silica it forms a meniscus. Some SiO_2 dissolves in the slag in the meniscus and this alters the surface tension (eg. $\gamma_{\text{SiO}_2} > \gamma_{\text{PbO}}$ but $\gamma_{\text{SiO}_2} < \gamma_{\text{FeO}}$) thus for the $\text{PbO} - \text{SiO}_2$ system the surface tension is greater at the tip than the base of the meniscus. Marangoni flow (surface-tension –driven flow) causes a flow from low to high surface tension so a flow is established which results in a vortex being formed; this vortex flow causes the gradual erosion of the refractory in this region [3]. The same mechanism applies to the $\text{FeO}- \text{SiO}_2$ slag but the direction of the slag flow will be the reverse of that for $\text{PbO}- \text{SiO}_2$.

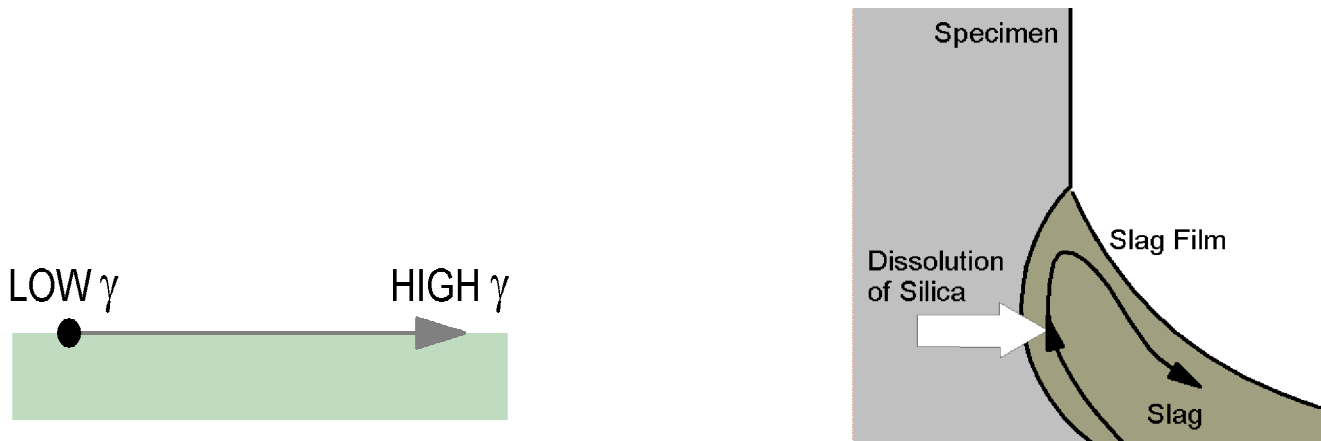


Figure 4: Schematic drawings showing (a) direction of Marangoni flow and (b) mechanism for slag line attack in PbO-SiO₂ slag [3]

In the case of the PbO- SiO₂ the slag film at the meniscus tip is higher than that at the base and the upward, Marangoni flow causes the slag to cover new refractory, this dissolves in the thin slag layer and creates a higher γ and so the slag is pulled further up to new area of refractory; this results in the slag creeping up the crucible and it will only flow back when the gravity force > upward Marangoni flow (Figure 5). This is known as *slag creeping*.

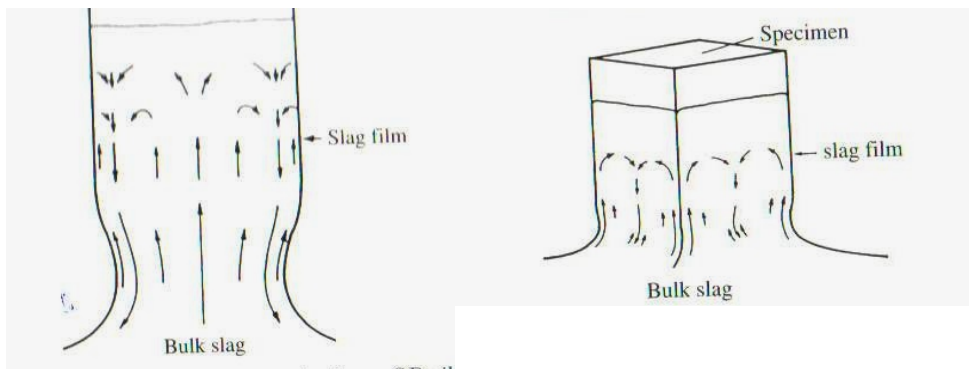


Figure 5: Schematic diagrams showing refractory erosion and creeping for PbO- SiO₂ for round and square-sectioned silica[3].

Mechanism of erosion in carbon/oxide refractories

Oxide refractories are prone to thermal shock. Modern refractories have much better thermal shock resistance through the addition of graphite particles, which absorb much of the stress generated by the expansion on heating of the oxide particles. The erosion/corrosion of these oxide/C refractories occurs by a different mechanism [3] to that for slag line attack. Figure 6 shows wetting and non-wetting conditions. At high temperatures *reactive wetting* is the norm *ie* wetting will occur when there is reaction (eg (i) oxide in the slag and (ii) C in the metal). If the refractory surface at any one time consists mostly of oxides, the conditions will favour the covering of the surface by slag (since the oxide is non-wetting to the metal but slag reacts with and “wets” the oxide). The slag will then gradually dissolve these oxide particles (Figure 7a). When the dissolution process results in a surface comprising mostly of graphite flakes the conditions become non-wetting to slag and the refractory is covered by metal since metal wets graphite. (Figure 7b) The dissolution of the graphite by the metal will occur until the majority of the surface is mostly covered by oxide (Figure 7a) at which point the metal will retreat and the surface will be covered by slag once more and then another cycle of dissolution will occur.

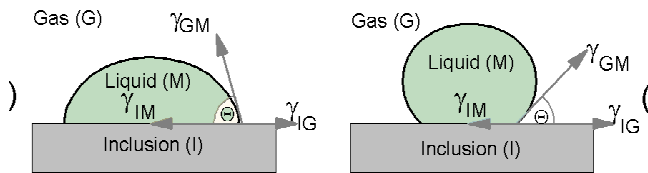


Figure 6: Schematic diagrams showing typical contact angles for wetting and non-wetting systems

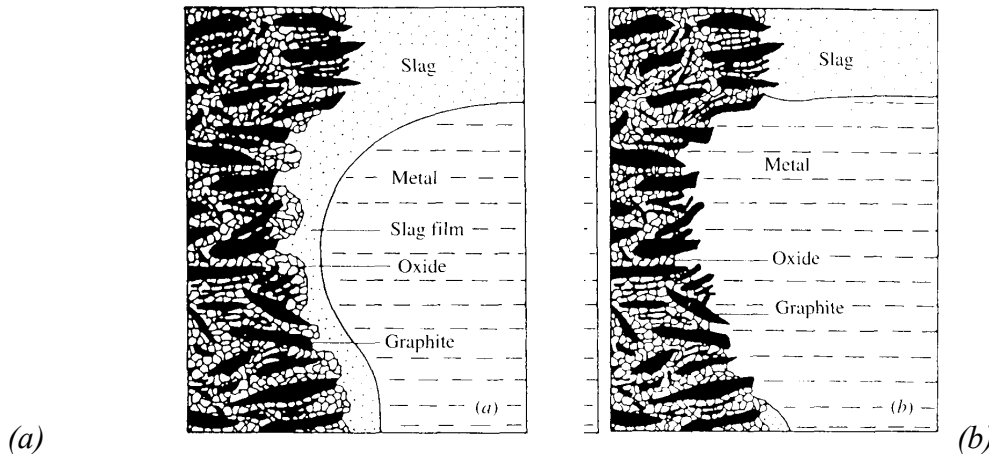


Figure 7: Schematic drawings showing the refractory erosion for Oxide/carbon refractories [3] where the refractory surface is predominantly (a) oxide and (b) graphite, respectively.

How to combat slag/erosion of refractories

The following methods are used:

- (i) Since erosion rates are directly related to the flow rates of the slag, then erosion rates can be reduced by (a) increasing the viscosity of the slag or (b) by reducing the flow rates of the metal (eg. by using electro-magnetic braking on the liquid metal) since these produce a drag force in the slag.
- (ii) The driving force for erosion is $(C_{sat} - C_o)$ where C_{sat} and C_o are the saturation concentration and actual concentrations, respectively; for ZrO_2 and ZrO_2/C refractories erosion can be decreased by adding 2% ZrO_2 to the slag to saturate it with ZrO_2 (for CC fluxes).
- (iii) It has been reported that making the slag non-wetting to refractory can extend refractory lives by the application of an electrical potential to the refractory and the slag [4,5].

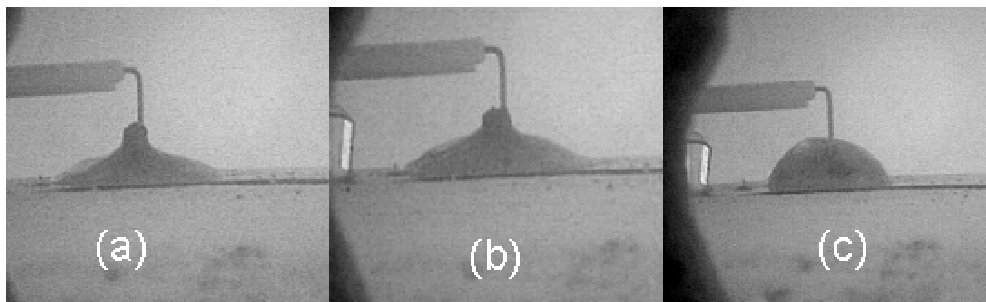


Figure 8: Effect of applying electrical potentials to a molten slag after 2 mins at (a) 0V (b) -1V and (c) -2V

(iv) ZrO_2 undergoes a high-temperature transition and is usually stabilised by CaO or Y_2O_3 ; it has been reported that CaF_2 attacks the stabilisers and promotes erosion [6].

(v) Creation of a **freeze lining** on the refractory surface; this is done by blowing the molten slag left in the vessel after draining the metal in order to produce a protective, consumable slag layer. **Slag splashing** is used in BOS practice; for successful slag splashing the FeO should equal ca 13% to get good adhesion with the refractory and the MgO % should be saturated (ca 8%) to create a high-temperature phase which slows down the erosion rate of the freeze lining [7].

1.1.2 Thermo-physical properties

We have seen above that thermo-physical property data are needed to (i) solve industrial problems with process control and improve product quality and (ii) the development of mathematical models of the process. These models often involve simulation of the fluid flow and heat transfer in the process and it has been shown that reliable predictions (for the process) require accurate data for the input data for the properties (eg. viscosity, density, thermal conductivity of the slag) [8]. Such measurements are frequently tricky because of the high temperatures involved and the consequent slag/container reactions. When you consider the large number of processes and the large number of properties required as input data, you soon realise that this is a massive job. This is further aggravated by the fact that compositions of reactants frequently vary. In mathematical modelling sensitivity analysis can ease this problem by indicating which property data are more important and the accuracy needed in such measurements. However, sensitivity analyses also show that the required accuracy required depends on what parameter is modelled eg. density may be required to 1% when modelling, say, porosity but, say, to 20% when modelling micro-structure. It is obvious that a large body of property values are needed for a wide range of slag compositions. Given the difficulties of making these measurements it follows what we need are models and routines which will calculate reliable and accurate property values from chemical composition since this available on a routine basis for most processes.

1.1.3 Estimation of thermo-physical properties

Various approaches have been used to derive estimated property values. These vary from at a simplest level to a numerical analysis of property values, for instance, analysis of T_{liq} as a function of chemical composition. More complex models relate the property to the structure of the slag and for the case of T_{liq} to phase diagram plus thermodynamic data for binary systems expressed as equations. Recently, models based on neural networks have been reported. The following should be noted:

- The accuracy of model predictions of properties can never be greater than that of the database; if the data are based on measurements from a single laboratory and contain a systematic error then the predicted values will also contain a systematic error.
- There are some discrepancies between the property values measured in different laboratories and thus a database based on such measurements will tend to be more scattered but will be applicable to a wider range of slags; the optimum condition is to use a database based on assessed property data.
- Models based on the structure of the slag which use one of the following (i) parameters such as (NBO/T) or the optical basicity (Λ) which can be calculated from the chemical composition or (ii) properties which are considered to represent the structure such as the excess free energy change ΔG^{xs} (since this is a measure of the strength of the bonding) or (iii) N_{O_0} , N_{O^-} , and N_{O_2} ie the number of BO, NBO and free-oxygens present.

Partial molar properties

Some properties (P) (such as C_p and ΔS^{fus}) are not affected much by the structure of the slag; in these cases, good estimates can be derived using the partial molar property values (P) using the Equation 5 where X= mole fraction (calculated by Equn 6) and 1,2 etc represent the slag components eg. SiO_2 , CaO etc. and M= Molecular weight of component = 60 for SiO_2 and $(\%)_1$ = mass % SiO_2 etc:

$$P = \sum \left[(X_1 \bar{P}_1) + (X_2 \bar{P}_2) + (X_3 \bar{P}_3) + (X_4 \bar{P}_4) \right] \quad (5)$$

$$X_{SiO_2} = X_1 = \{(\%)_1 / M_1\} / [\{(\%)_1 / M_1\} + \{(\%)_2 / M_2\} + \{(\%)_3 / M_3\} + \{(\%)_4 / M_4\} + \dots] \quad (6)$$

The values for P_T are those for the pure component (eg. SiO_2) for the temperature of interest.

2. The Structure of slags

2.1 Structure of slags and glasses

The structure of SiO_2 is a 3D array (Figure 9a,b) with (i) each Si^{4+} surrounded by 4 O^{2-} arranged tetrahedrally and (ii) and each O^{2-} connected to two O^{2-} (denoted **bridging O**) which causes the formation

of a 3-D array. Cations eg Na^+ or Ca^{2+} break the chain by forming a bond, $\text{O}^{2-} \text{--} \text{Na}^+$ (denoted **non-bridging O**). The methods used to determine structure are summarised in Appendix 1. Slags and glasses are polymers in the form of chains, rings etc made up of SiO_4^{4-} tetrahedral units (Figures 9,10). They have the following characteristics [9-12]:

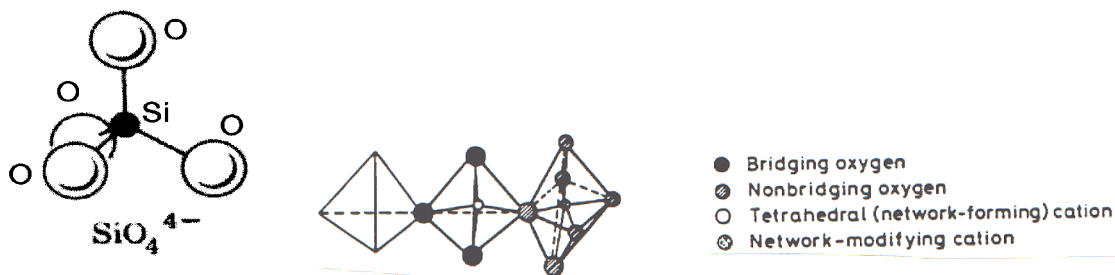


Figure 9: Structure of SiO_2 showing 3-D characteristics

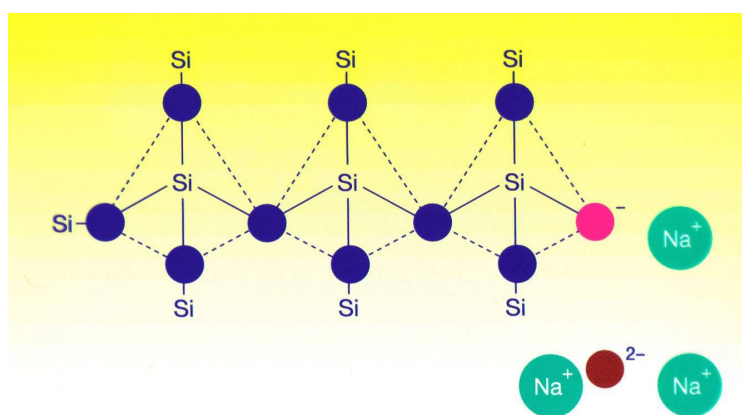


Figure 10. Schematic drawings and silicate chain with Bridging O (O^0) shown in black, non-bridging O (O^-) as free O^{2-} as green.

- Each Si (with a valence of 4) is surrounded (tetrahedrally) by 4 O^{2-} ions (with a valence of 2) each connecting to 2Si ions (Figure 9)
- In SiO_2 these SiO_4^{4-} polyhedra are connected in a 3-dimensional polymerised structure (Figure 9b, 10) and the oxygens are predominantly **bridging oxygens** (denoted O^0).
- Cations such as Ca^{2+} , Mg^{2+} etc. tend to break up the Si-O bonds and de-polymerise the melt by forming **non-bridging oxygens** (NBO denoted O^-) and **free oxygens** (denoted O^{2-}) i.e. not bound to Si at all but to Na^+ etc (Figure 10).
- Other cations such as Al^{3+} , P^{5+} , Ti^{4+} can fit into the Si polymeric chain but need to maintain charge balance e.g. if an Al^{3+} is incorporated into a Si^{4+} chain it must have a Na^+ (or one half¹ of a Ca^{2+}) sitting near the Al^{3+} to maintain local **charge balance** (Figure 11). In practice, Ti^{4+} has been reported (on the basis of viscosity measurements [13]) to act as a network breaker (ie is in 6-fold coordination) and has been treated as such in this work.
- Smaller cations such as Mg^{2+} tend to give a wider distribution of chain lengths than larger cations such as Ba^{2+} .
- Cations such as Fe^{3+} in small concentrations can act as network breakers but in higher concentrations can be incorporated into the chain in a similar way to Al^{3+} .

¹ The Ca^{2+} would charge balance two neighbouring Al^{3+} ions

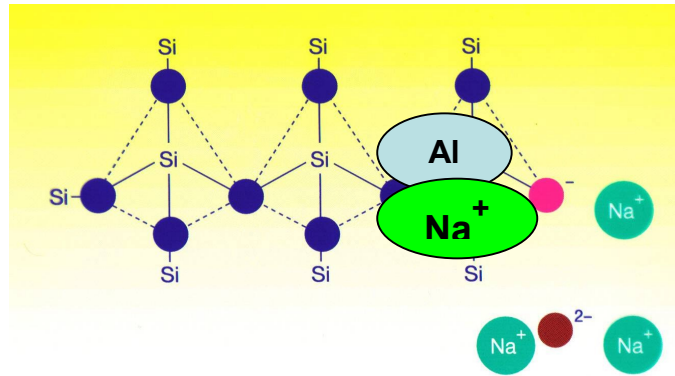


Figure 11: Schematic drawing showing Al^{3+} incorporated into silicate (Si^{4+}) chain, which requires cation (shown here as Na^+) to maintain charge balance

- The degree of polymerisation can be expressed in terms of the numbers of **bridging** (N^{O_0}) **non-bridging** (N^{O^-}) and **free- oxygens** ($N^{O^{2-}}$). However the degree of de-polymerisation is frequently represented by parameters such as the ratio of {NBO/T (the ratio of the number of non-bridging O atoms to O atoms in tetragonal co-ordination)} which is denoted **(NBO/T)** [9-12] or the optical basicity (Λ) [12].
- The structure of melts (both slags and metals) can be represented using thermodynamic quantities (e.g. excess free energy [14,15]) since thermodynamics provides a description of bond strengths.
- B^{3+} has 3 fold coordination in borosilicates but the structure of borosilicates (used as enamels) is a complex mixture of 3- and 4- co-ordination [16,17].
- The structures of glasses are very similar to those of liquid slags [18].
- Some metallurgical slags have a high basicity (e.g. $CaO/SiO_2 > 2$) and consequently the Si^{4+} ions are predominantly in the form of monomers *i.e.* completely de-polymerised.

2.2 Parameters used to represent structure

2.2.1 NBO/T and Q

NBO/T= number of **non bridging O** / **tetragonally –bonded oxygen**

(NBO/T) is a measure of the de-polymerisation and can be calculated using the procedures listed below. However, cations like Na^+ or Ca^{2+} act as network –breakers but if an Al^{3+} goes into the chain it requires a cation eg Na^+ to be sited near Al^{3+} to provide charge balance (Figure 11). **A cation on charge-balancing duties cannot be used as a network- breaker.** The parameter, **(NBO/T)_{corr}** is a measure of the de-polymerisation of the slag. (NBO/T)_{corr} can be calculated in the following manner where f= fraction of Fe^{3+} ions acting as a network breaker:

1. Calculate

$$Y_{NB} = \sum 2 [X_{CaO} + X_{MgO} + X_{FeO} + X_{MnO} + X_{CaO} + 2X_{TiO_2} + X_{Na_2O} + X_{K_2O} + 3f X_{Fe_2O_3} - 2X_{Al_2O_3} - 2(1-f)X_{Fe_2O_3}] \quad (7)$$

2. Then calculate $X_T = \sum X_{SiO_2} + 2 X_{Al_2O_3} + 2 f X_{Fe_2O_3} + \dots$ (8)

3. $(NBO/T)_{corr} = Y_{NB} / X_T$

4. **Q** is a measure of the polymerisation of the slag and for this reason is often preferred to (NBO/T)
 $Q = 4 - (NBO/T)$ (9)

Table 1: NBO/T and Q for various CaO- SiO₂ slag compositions

		NBO/T	Q	
SiO ₄ ⁴⁻ (monomer)	2CaO.SiO ₂	4	0	BOS slag
Si ₂ O ₇ ⁶⁻ (polyhedra)	3CaO.2SiO ₂	3	1	Mould flux; billets; Q= 1
Si ₂ O ₆ ⁴⁻ (chain)	CaO.SiO ₂	2	2	BF slag Q>2 Mould flux; Q= 2.5
Si ₂ O ₅ ²⁻ (sheet)	CaO. 2SiO ₂	1	3	Glasses, Coal slags
SiO ₂ (3-dim)	SiO ₂	0	4	Glasses

2.2.2 Optical basicity(Λ)

One problem encountered with both (NBO/T) and Q is that they do not differentiate between the effects of different cations on the silicate structure. The optical basicity (Λ) has been used as a measure of structure' principally because it does provide some measure of differentiating between different cations. It can be calculated in the following manner:

$$1. \Lambda = \frac{\sum (X_1 n_1 \Lambda_1 + X_2 n_2 \Lambda_2 + X_3 n_3 \Lambda_3 + \dots)}{\sum (X_1 n_1 + X_2 n_2 + X_3 n_3 + \dots)} \quad (10)$$

where n = number of oxygens in oxide eg n=2 for SiO₂ or 3 for Al₂O₃

2. Λ^{corr} is calculated by deducting the mole fraction of cation required to charge balance the Al³⁺ in the chain, this is usually deducted from the largest cation present eg. Ba²⁺ thus $X^{corr}_{BaO} = (X_{BaO} - X_{Al_2O_3})$

The following values of optical basicity are recommended:

Al₂O₃= 0.60: B₂O₃= 0.42: BaO=1.15: CaO= 1.0: FeO= 1.0: Fe₂O₃= 0.75: K₂O= 1.4; Li₂O= 1.0: MgO= 0.78: MnO= 1.0: Na₂O= 1.15: P₂O₅= 0.40: SiO₂= 0.48: SrO= 1.10:TiO₂= 0.61:

Various Λ values have been cited for CaF₂ 0.43, 0.67 but a value of 1.2 should be used for viscosity calculations. However, recent work due to Sasaki et al. [19] indicates that Ca²⁺ bonds with 2F⁻ and thereafter is "out of the game" (thus one can correct the slag composition by ignoring F concentration and deducting 2X_F from X_{CaO})[20]

2.3 Structural changes in glasses and slags with temperature

When a glass or a glassy slag (Q> ca.2 .5) is heated both C_p and thermal expansion (and other properties, eg. k) measurements show a marked change at a specific temperature (as can be seen in Figure 12); this is called the **glass transition temperature** (T_g). The change in C_p and α is due to the glass transforming into a super-cooled liquid (but which appears to be a solid). This super-cooled liquid (scl) exists until the slag melts into a true liquid. However, some slags (with lower Q say <2) the scl undergoes crystallisation which is an exothermic transition. On heating, the following changes in glassy slag properties occur at T_g (i) a step increase in C_p with C_p of the glass remaining higher than that of the crystalline slag over the entire range between T_g and T_{liq} (ii) a three-fold increase in thermal expansion (iii) a remarkable decrease in viscosity with increasing temperature, the following value is frequently cited, η (dPas)=10^{13.4} at T_g and (iv) an abrupt decrease in the slope of k as a function of temperature .

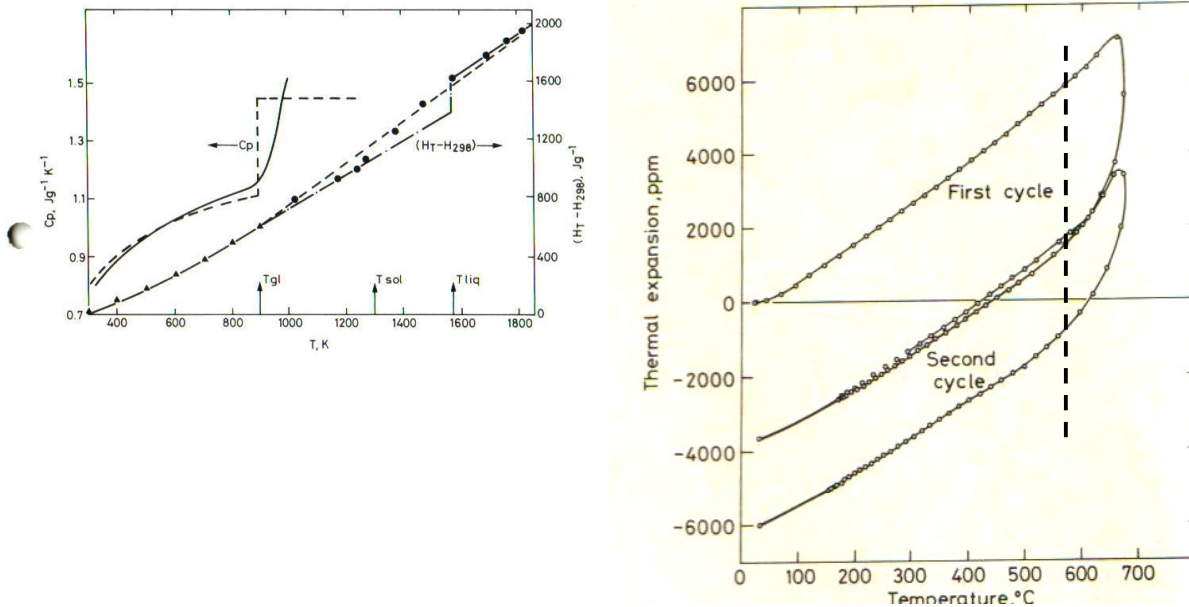


Figure 12: (a) Heat capacity for a glassy slag and (b) Thermal expansion coefficient as a function of temperature.

Viscosity (η) measurements on glassy samples ($Q > 2.5$) carried out whilst cooling show viscosities (i) with higher values than that of a less-polymerised sample ($Q = 2$) and (ii) a smooth change with temperature as the liquid transforms to scl (with $\eta = 10^{12.4}$ Pas at T_g). It can be seen from Figure 13b that viscosities for less polymerised slags ($Q < 2$) show a sharp change in slope (at the *break temperature*, T_{br}) when crystalline materials are first precipitated; it should be noted T_{br} decreases as the cooling rate increases.

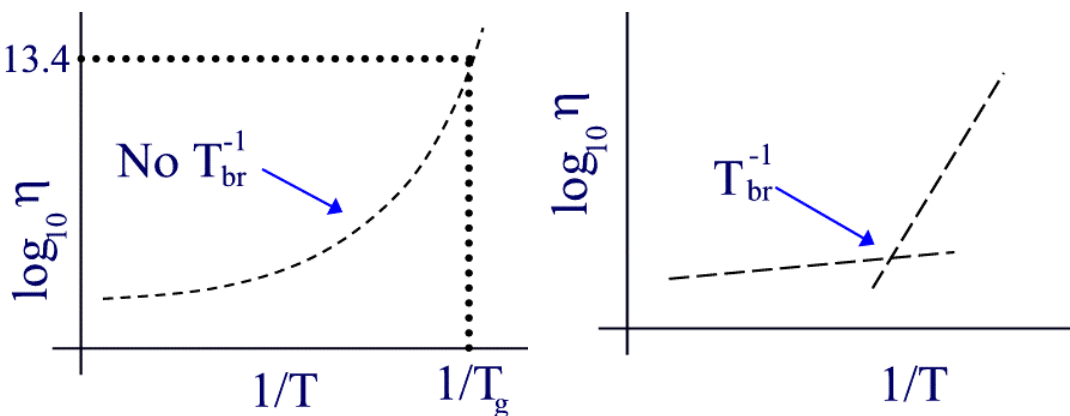


Figure 13: Plots of \log_{10} viscosity as functions for reciprocal temperature (K^{-1}) for (a) glassy slag ($Q > 2.5$) and (b) for a less-glassy slag ($Q = 2$).

2.4 Effect of structure on properties

The effect of polymerisation (or Q) on property values are arranged so the properties showing the biggest dependence on structure first and with diminishing dependence on structure as we go down

2.4.1 Effect of structure (Q or (NBO/T)) on properties

Property values for slags and glasses are greatly affected by the degree of polymerisation (ie. Q); polymerisation (or Q) increases as (i) SiO_2 and Al_2O_3 (**network-former**) concentrations increase and (ii) Na_2O , Li_2O , CaO , MgO , K_2O , SrO and BaO (**network-breakers**) decrease.

Viscosity (η)

Viscosity involves transporting one layer of liquids over another; thus the longer the chain length (or polymerisation) the more difficult this task becomes. It can be seen from Figure 14a that the viscosity

shows a dramatic decrease between NBO/T=0 and 1 (or Q= 4 to 3) If we need to represent the structure through a property, the viscosity is the best property to represent the structure of the glass .

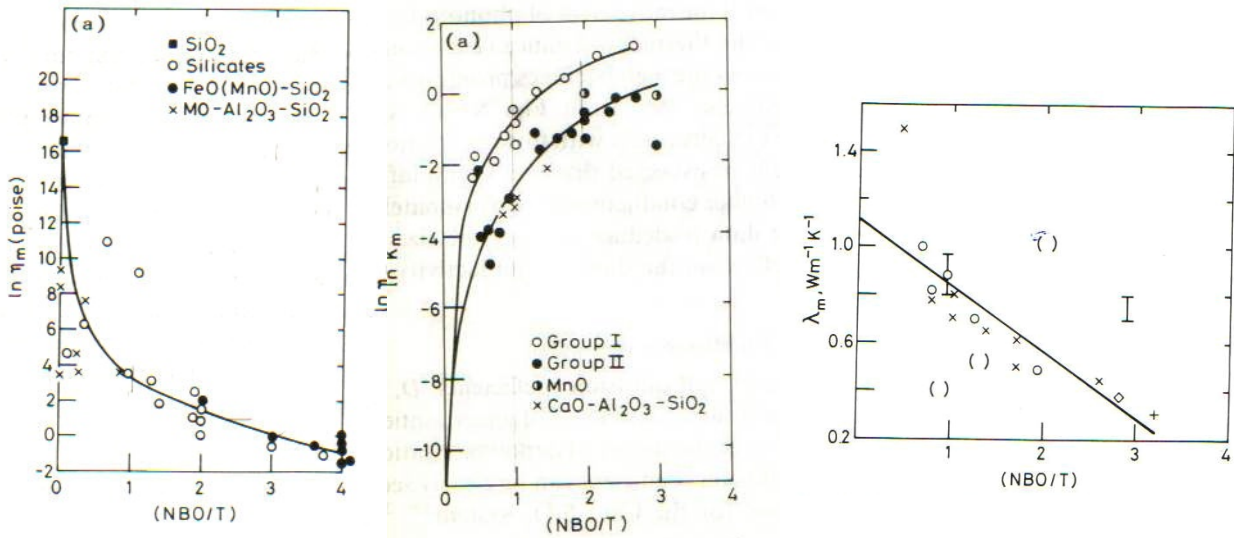


Figure 14 (a) Viscosity (b) Electrical conductivity and (c) Thermal conductivity as functions of (NBO/T) of liquid slags at T_{liq} [12]

Thermal conductivity (k) and electrical conductivity (κ)

The **thermal conductivity** of liquid slags tends to increase with increasing SiO₂ content; this can be seen in Figure 14c where the thermal conductivity (k) decreases with increasing NBO/T (or decreasing Q). Thermal conductivity is high for covalently- bonded Si⁴⁺ and Al³⁺ ions in the chain but is much lower for the NBO and cations at the end of chains. This can be expressed as conduction is easy along the chain (ie. thermal conductivity is much larger) but the transport of phonons is much more difficult for chain-to-chain movement. The thermal conductivity seems to be affected by the nature of the cations with $k_{Li_2O} > k_{Na_2O} > k_{K_2O}$.

Electrical conductivity involves the movement of cations through a silicate network when an electrical field is applied; thus a well-developed network will hinder their movement of these cations. It can be seen can be seen from Figure 14b that κ increases sharply (i) as NBO/T increases (or Q decreases) and (ii) when Mg²⁺, Ca²⁺, Sr²⁺ and Ba²⁺ are replaced by Li⁺, Na⁺, or K⁺. Consequently, there are two factors affecting electrical conductivity (i) the degree of polymerisation of the slag with the electrical resistivity (1/κ) increasing as polymerisation (Q) increases and (ii) the size and concentration of the cations since the number of cations slipping through the “holes” in the network will be greater for high concentrations of cations and for smaller cations.

Thermal expansion(α,β) and density (ρ)

SiO₂ has a very low **thermal expansion coefficient** because of the tight bonding. First order properties (eg $\alpha \equiv dp/dT$ shown in Figure 15a) tend to be more sensitive to temperature than the property itself (eg. ρ) ; the density is only slightly sensitive to the polymerisation (Q) in the slag. It can be seen from Figure 15a that thermal expansion (1) increases with increasing NBO/T (or decreasing Q) and (2) is greater for M₂O than MO and that increases with increasing cation size (K>Na>Li and Ba>Ca>Mg). In Figure 15b it can be seen that there is a marked change in thermal expansion when T>T_g (ca. 300%) which occurs when the glass changes into a scl. However, accurate values of thermal expansion of glassy slags are difficult to obtain for T>T_g because the super-cooled liquid tends to collapse under the pressure of the probes.

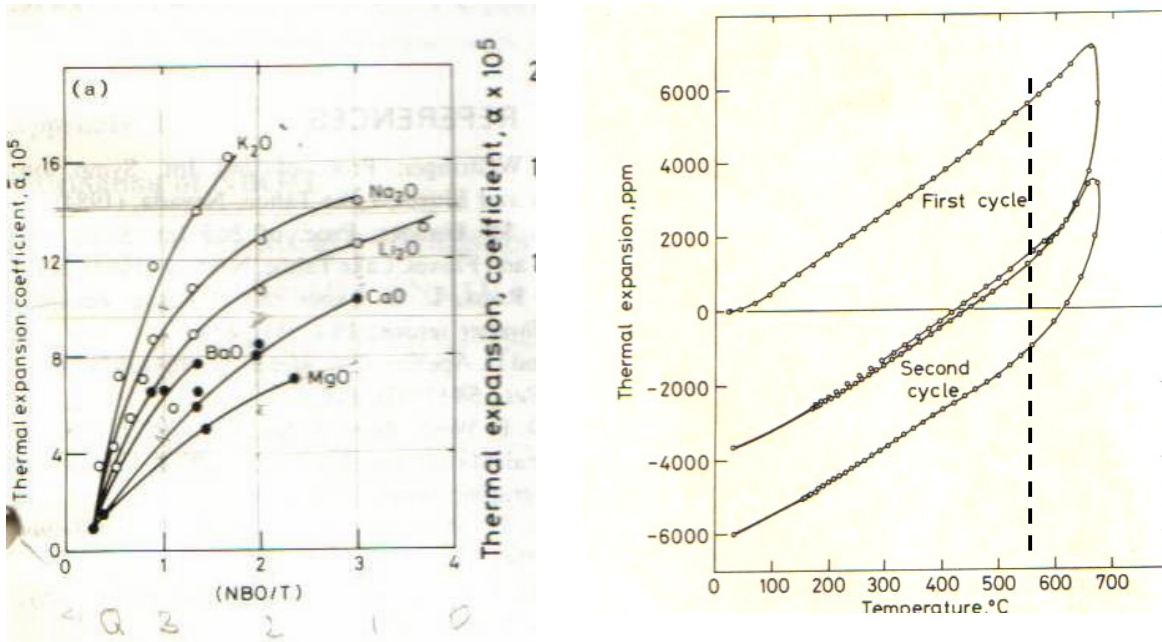


Figure 15: Thermal expansion of (a) liquid binary slags as a function of (NBO/T) and (b) increase in expansion of solid (note change of slope at T_g)

Surface tension (γ) and emissivity (ϵ)

These properties predominantly depend on the surface and not the bulk. In mixtures, the constituents with the lowest **surface tension** (called “*surfactants*”) will tend to occupy the surface layer (eg. S in steels and *surfactants* like B_2O_3 in slags). The surface concentration will depend upon both surface tension and the chemical activity of the component (eg B_2O_3 in the slag). When there are two or more, surface-active components in the slag (eg CaF_2 and B_2O_3) there will be competition for the surface sites. The surface tension is a thermodynamic property. Surface tensions of some oxides are given in Table 2 since $\gamma_{SiO_2} > \gamma$ for other oxides it follows that γ will decrease with increasing SiO_2 and increasing Q.

Table 2: Surface tensions (mNm^{-1}) of pure slag components at 1773K

	SiO_2	CaO	BaO	SrO	MgO	Al_2O_3	MgO	FeO	NiO	MnO	CrO	Na_2O	K_2O	TiO_2	ZrO_2	Cr_2O_3	Fe_2O_3	CaF_2	B_2O_3
γ	260	625	560	600	635	655	635	645	645	645	360	295	160	360	400	800	300	290	110

Slags and glasses are semi-transparent to IR radiation. Slags and glasses are optically- thick if $\alpha^*d > 3$ where α^* =absorption coefficient. In practice, this means the **emissivity** of liquid slags will depend on the depth of the slag sample. Values are usually cited for the *optically thick condition*.

Heat capacity (C_p), entropy of fusion (ΔS^{fus})

These properties are little affected by structure and Equations 6 and 7 are valid , where 1,2 etc represent the different components, eg. SiO_2 etc. However, C_p is dependent upon the nature of the slag and C_p jumps abruptly at T_g when a glass changes to a scl whereas a crystalline slag (1) shows no jump at T_g (2) $C_{p\ scl} > C_{p\ cryst}$ over the range T_g to T_{liq} and (3) exhibits an enthalpy of fusion (ΔH^{fus}) at T_{liq} whereas a scl exhibits no ΔH^{fus} .

$$P = \sum \left[(X_1 \bar{P}_1) + (X_2 \bar{P}_2) + (X_3 \bar{P}_3) + (X_4 \bar{P}_4) \right] \quad (6)$$

2. Types of Model

Several types of models have been reported for calculating the properties of slags; these are classified into five groups ie. 1. Numerical fits 2. Neural network models 3. Partial molar models 4. Models based on structural parameters 5. Thermodynamic models (which take structure into account) and 6. Molecular Dynamics (MD) models. These are summarised below.

3.1 Numerical fits

With these an experimental database is established covering the compositions of the slags and the property being modelled eg. liquidus temperature, T_{liq} . A numerical analysis is then carried out to obtain the “best fit” in which T_{liq} is represented as $C_1(\text{comp}_1) + C_2(\text{comp}_2) + C_3(\text{comp}_3) + \dots$ where C is a constant, comp =either % or X and 1,2,3, =different components eg. SiO_2 etc. One problem with this approach is that unrealistic constants can be recorded for components in low concentrations (eg. K_2O in mould fluxes) and it is frequently better for this case to add the % (or X) K_2O to % (or X) Na_2O which is present in greater amounts and exhibits similar behaviour.

This approach is more successful when applied to a family of slags (eg. mould fluxes or ferro-chrome slags) with limited compositional range than for a wide range of slag compositions which involve complex and very different phase equilibria. Some typical applications are for T_{liq} and T_{br} of mould fluxes which allow values to be calculated to better than $\pm 30\text{K}$ to be calculated [21].

$$T_{liq}(\text{K})=1464+ 11.4\%\text{SiO}_2-11\%\text{CaO} +4.2\% \text{Al}_2\text{O}_3+5.7\%\text{MgO}-10.1\%\text{Na}_2\text{O} -15.8\%\text{K}_2\text{O} +1.9\%\text{F} +8.3\%\text{Fe}_2\text{O}_3 +11.6\%\text{MnO} \quad (11)$$

$$T_{br}(\text{K}) = 1393- 8.4\% \text{Al}_2\text{O}_3- 3.3 \%\text{SiO}_2+ 8.65\%\text{CaO}-13.86\% \text{MgO} -18.4\%\text{Fe}_2\text{O}_3 -3.2\% \text{MnO} -9.2\%\text{TiO}_2- 2.2\%\text{K}_2\text{O} -3.2\%\text{Na}_2\text{O} -6.47\% \text{F} \quad (12)$$

3.2 Neural network models

The human brain contains $>10^{10}$ cells (“neurons”) in a neural network consisting of several (3 here) layers. When units are inserted into “input layer” they are transmitted to the “middle layer” and when the intensity exceeds a critical value they are transmitted on to the “output layer” (Figure 16). Signal transmission is represented by a sigmoidal function in the software. In the output layer the output values are (i) compared with teaching values (ie experimental values fed previously) and (ii) errors are computed. These errors are then transmitted back to the nodes between layers to re-calculate the weights. These procedures are called “learning” and learning is repeated until the target attained or errors are within acceptable limits. In the studies of Nakamoto [22, 23] the teaching value is “measured viscosity” and the input values are temperature and compositions of the slags. Neural network models have been used to calculate the viscosities of (i) ferro-chrome ($\text{CaO}+\text{Al}_2\text{O}_3+\text{MgO} +\text{CrO}_x+\text{SiO}_2$) slags [22] see Figure 17 and (ii)mould fluxes [23] which available commercially. Nakamoto et al [22] report uncertainty values for the function $\{100(\eta^{\text{meas}}-\eta^{\text{calc}}/\eta^{\text{meas}})\}$ were $\pm 22\%$ for ferro-chrome-type slags. Neural network values have also been used to determine surface tension [78] and Sulphide capacities.

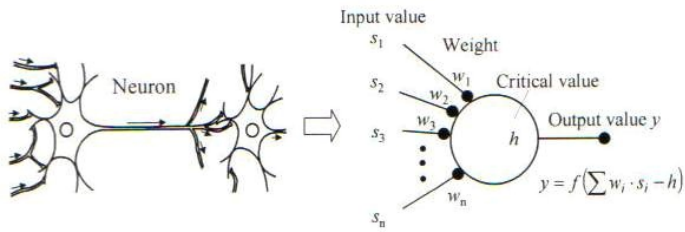


Figure 2: A concept of neuron model

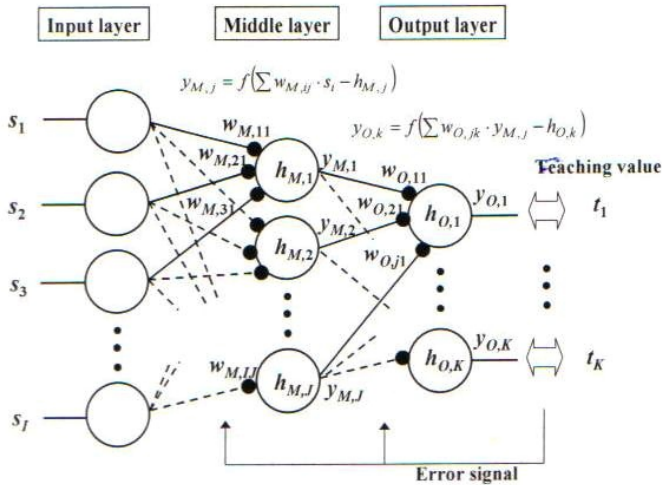


Figure 16: Schematic diagrams illustrating (i) concept of neuron model and (ii) neural network.

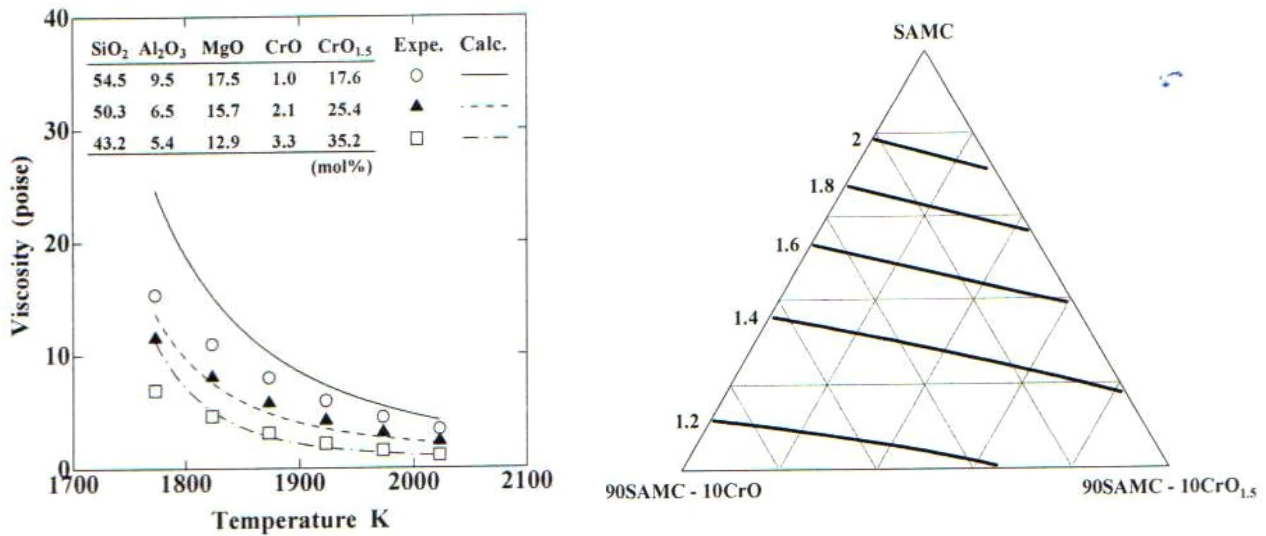


Figure 17: (a) Viscosity as a function of temperature for a MgO+CrO+CrO_{1.5}+Al₂O₃+SiO₂ slags and (b) Iso-viscosity (dPas) contours for a Fe/Cr process slag at 1923K SAMC = (X_{MgO} = 0.41) + (X_{CaO} = 0.074) + (X_{SiO₂} = 0.343) + (X_{Al₂O₃} = 0.173) [22]

3.3 Models based on structure

The majority of reported models take the structure into account. Earlier models tended to use basicity (eg. CaO/SiO₂) ratios to represent the structure. The widely used Riboud model [24] classifies oxides into 5 groups “CaO” “SiO₂” “Al₂O₃” “Na₂O” “CaF₂” which are network-breakers or network-formers. More recent models have tended to use one of the following parameters used to represent structure (NBO/T or Q; optical basicity, or the number of Bridging or- Non- bridging and free-O, (N_{O0}, N_{O-}, and N_{O2-}, respectively). Details of these parameters are given above in Section 2.2

3.4 Thermodynamic models

There are several commercial thermodynamic models available (eg. MTDATA [25], Thermocalc, [27] Factsage [26]). These models are based on database of phase equilibrium and thermodynamic data for various binary systems eg. CaO- SiO₂; FeO- SiO₂; etc. In the case of MTDATA [28] for instance the liquid CaO-SiO₂ system is considered to be made up species CaO and SiO₂ and by “associate species” such as CaSiO₃ and Ca₂SiO₄. Polynomial equations are used to represent these data for these species and to account for sharp changes in thermodynamic properties at specific compositions (eg. where miscibility gaps occur). Equations for binary systems are used to predict the equilibrium phase diagrams and chemical activities, free energies, enthalpies, C_p and T_{liq} and T_{sol} values for ternary, quaternary and higher systems. Most crystalline phases are assumed to mix independently on a series of separate sub-lattices. In recent years, these commercial models have been extended to the calculation of physical properties such as densities, viscosities and surface tensions of slag systems. Properties such as viscosity involve the movement of one liquid, slag particle over another and this is related to the strength of the bonding and thermodynamics provides a measure of the strength of the bonding.

Thermodynamic models involve:

- An extensive database of phase equilibrium data and thermodynamic properties which have been assessed to provide reference data for the various binary-, ternary –etc.; These evaluated data are represented as polynomial equations in terms of T, and used to calculate data for ternary and higher systems
- The principal differences between specific models lie in the different ways the liquid is represented eg MTDATA use the *associate species model* for the liquid

There are differences in the approaches taken to model physical properties, such as viscosity, in the various models. For instance in model due to Zhang et al [29,30] the values of N_{Oo}, N_{O-}, and N_{O2-} are first calculated using the Kapoor-Frohberg cell model (as developed by Gaye et al [31]) and then fitting constants a, b, c, d, a' and b' are derived for each binary system. Viscosity values for ternary and higher systems are calculated using the fitting constants for the binary systems (Eqns13-16) but adjustments are needed in some cases. These quantities are then used to calculate ln A and B for the Weymann equation(Eqn 13). The software is commercially available.

$$\eta = A_w T \cdot \exp(E_w/R^*T) \quad (13)$$

$$E_w = a + b(N_{Oo})^3 + c(N_{Oo})^2 + d(N_{O2-}) \quad (14)$$

$$\ln A_w = a' + b' \cdot E_w \quad (15)$$

$$a = \sum X^i a^i \quad (16)$$

where E_w=activation energy, R*=Gas constant and a, b, c, d =fitting constants .

Tanaka et al.[15] also use the Kapoor Frohberg cell model to calculate the N_{O-} and N_{O2-} and the Arrhenius equation and $E\eta = E / 1 + \{ \sum \alpha_i^* (N_{O-} + N_{O2-}) \}^{0.5}$ where A and the constants, α_i* are determined from experimental viscosity data.

In contrast, Seetharaman and Du [32,33] adopt a very different approach. The effect of structure is determined as thermodynamic function (Equn 17) where ΔG* =free energy of individual components 1,2 etc, ΔG_η^{mix} = free energy of mixing and 1,2=components eg. CaO.

$$\Delta G^*_{\eta} = \sum \Delta G^* + \Delta G_{\eta}^{\text{mix}} + 3R^*T X_1 X_2 \quad (17)$$

The viscosity is then calculated using Equn 18 where h=Planck Constant and N_A=Avogadro number thus A_A =hN_Aρ/ M and B_A= ΔG*_η.

$$\eta = hN_A \rho / M \exp(\Delta G_{\eta} / RT) \quad (18)$$

Although thermodynamic models may provide reliable thermodynamic values, the accuracy of the viscosity prediction will lie in how well the selected thermodynamic functions represent the effect of structure on the viscosity. This model has been adopted by other groups [40].

3.5 Molecular Dynamics (MD) models

Molecular dynamics (MD) is a computer simulation where molecules are allowed to interact for a period of time and which is approximated by using the physics of particle motion. MD is based on Statistical Mechanics and makes use of Potential Energy functions to calculate bonding characteristics and motion of the molecules from which the viscosity and self-diffusion of O, Ca, Si, F can be determined. The accuracy of MD calculations is limited by the accuracy of Potential Energy functions for many silicate systems. MD calculations of bonding characteristics and slag viscosities have been reported by Zhang et al [35] and by Ogawa et al. [36] and for Diffusion coefficients by Asada et al.[20]

4. Modelling physical properties

4.1 Liquidus (T_{liq}) and solidus (T_{sol}) temperatures

The various commercial models available are capable of calculating reliable values of T_{liq} and T_{sol} for multi-component slags over large compositional ranges..

However, it is difficult to calculate values of T_{liq} and T_{sol} for wide ranges of composition and it may be necessary to make experimental measurements for the calculation of estimated properties. However, it may be possible to estimate T_{liq} and T_{sol} for a specific family of slags (for instance mould fluxes) by creating a database of T_{liq} and T_{sol} and correlating these with their chemical compositions to obtain “best fit” constants. Examples of this approach are determination of T_{liq} and T_{br} of mould fluxes from measured values and chemical composition data [21]. Care must be taken with the constants derived for constituents (eg K₂O), which occur in low concentrations since the residuals in the calculations tend to get dumped onto these materials leading to unrealistic constants. In these cases more appropriate constants can be derived by adding the material to a similar material (eg K₂O + Na₂O).

$$T_{liq}(K)=1464+ 11.4\%SiO_2-11\%CaO +4.2\% Al_2O_3+5.7\%MgO-10.1\%Na_2O -15.8\%K_2O +1.9\%F +8.3\%Fe_2O_3 +11.6\%MnO \tag{11}$$

$$T_{br}(K) = 1393- 8.4\% Al_2O_3- 3.3 \%SiO_2+ 8.65\%CaO-13.86\% MgO -18.4\%Fe_2O_3 -3.2\% MnO -9.2\%TiO_2- 2.2\%K_2O -3.2\%Na_2O -6.47\% F \tag{12}$$

The principal methods of determining T_{liq} are (i) DTA/DSC [37,38] (ii) single and double high-temperature thermocouple methods [39] and (iii) quenching slag samples in Pt capsules from different temperatures followed by metallographic examination to identify melting in the sample .For accurate values the following procedures should be adopted: (i) DSC measurements should be conducted in the heating cycle since significant under-cooling can occur in cooling (ii) the measurement thermocouples should be calibrated using standard reference materials appropriate for the slag samples (eg metals have significantly higher thermal conductivities than slags) (iii) measurements should be carried out using different heating and extrapolated to zero heating rate to determine the magnitude of the correction term.

4.2 Heat capacity, enthalpy

Factors affecting property: The heat capacities of slags are little affected by the structure of the slag; thus it is possible to obtain reasonable estimates of C_p from partial molar C_p values for individual components (eg where 1, 2= CaO, SiO₂ etc).

$$C_p = \Sigma (X_1C_{p1}) + (X_2C_{p2}) + (X_3C_{p3}) +(X_4C_{p4}) \tag{19}$$

It is customary to express the temperature dependency of C_p in the form of:

$$C_p =a + bT -c/T^2 \tag{20}$$

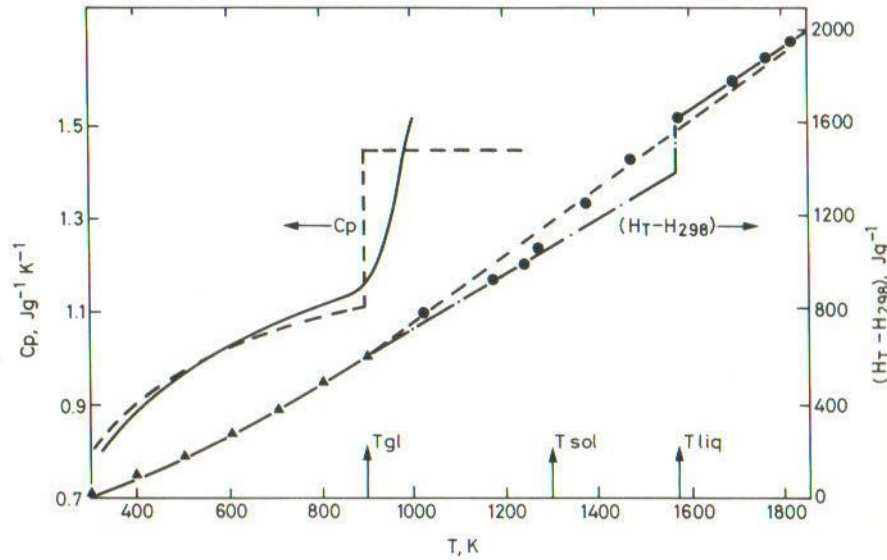


Figure 18: Schematic representation of heat capacity and enthalpy ($H_T - H_{298}$) of glassy and crystalline slag phases.

Measurement methods

Various methods are available for measuring C_p and $(H_T - H_{298})$; descriptions of these methods have been given elsewhere [37,38]. The most popular methods today are differential scanning calorimetry (DSC) and drop calorimetry; the experimental uncertainty for both of these methods is ca $\pm 2\%$. More accurate C_p values can be derived from $(H_T - H_{298})$ values obtained from drop calorimetry with C_p values measured using DSC [38]. It should be noted that cooling rates are very high in drop calorimetry, which will promote the formation of glassy phases.

Different models available in literature

Thermodynamic models derive C_p and enthalpy values from differentiation of ΔG data for the slag [40]. Less accurate derived (uncertainty $\pm 2-5\%$) can be derived from the method described above (Eqns 19 to 24). The major uncertainty in any estimate lies in the degree of crystallisation of the sample which occurs in the T_g to T_{liq} range and which may be significantly different for industrial conditions from that for DSC conditions.

4.3 Thermal expansion

The thermal expansion is frequently expressed through by the volume (β) and linear thermal expansion coefficients (α) which are given in Eqns 25 and 26 where $\beta_{(298-T)}$ and $\alpha_{(298-T)}$ are the volume and linear coefficients, respectively and V_0 , L_0 =volume or length of sample at the reference temperature (T^{ref}), usually 293 or 298K for the solid and T_{liq} for the liquid.

$$\beta_{(298-T)} = \{(V_T - V_0) / V_0 (T - T^{ref})\} \quad (25)$$

$$\alpha_{(298-T)} = \{L_T - L_0\} / \{L_0 (T - T^{ref})\} \quad (26)$$

The linear thermal expansion is frequently presented as $\Delta L\%_T$ since densities are readily calculated by Eqns 27 and 28 where L_0 and ρ are the length and density at the reference temperature (T^{ref}) ie 298 or 293 K for the solid and $T^m (=T_{liq})$ for the liquid:

$$\Delta L\%_T = 100 (L_T - L_0) / L_0 \quad (27)$$

$$\rho_T = \rho_0 / [1 + \{0.01 \Delta L\%_T\}]^3 \quad (28)$$

Factors affecting property: Thermal expansion parameters (α , β and $\Delta L\%_T$) are very dependent upon structure since the thermal expansion is very low for SiO_2 with its highly polymerised 3-D network (Figure 15a); thus thermal expansion parameters will decrease as Q (polymerisation) in the slag increases.

The transition of glass to scl at T_g is associated with a large increase in α as shown in Figure 15b ($\alpha_{T>T_g} \approx 3\alpha_{T<T_g}$). However, it is quite difficult to obtain thermal expansion data for the scl phase since the pressure of the probes on the specimen in a dilatometer results in a collapse of the sample for the scl phase.

Measurement methods

At room temperature the density of slags can be measured by accurate measurements of the sample mass and its dimensions. However, it is usually preferable to use the Archimedian method which entails measuring the apparent loss of weight of the sample when immersed in distilled water.

At higher temperatures the following methods are frequently used (i) dilatometry (ii) Archimedian method where a probe (or bob) is immersed in the molten slag. (iii) sessile drop where the volume of the drop is determined (iv) pycnometry (v) Maximum bubble pressure (MBP) method where the density is determined through MBP measurements at different immersion depths [43, 37] The experimental uncertainty is usually in the range $\pm 1-2\%$.

4.4 Density (ρ)

The density is derived directly in thermodynamic models [40].

Persson [41] et al estimated molar volumes (V) by the following equation where the superscript M and subscript m refer to the integral and partial molar quantities and H refers to the enthalpy of mixing and λ is a constant; the values of ΔG , λ and interaction coefficients were derived from their thermodynamic model:

$$V^M / \sum X_i V_m = \lambda H^M / RT \quad (29)$$

It is possible to derive reasonably accurate density values from a simpler model since the densities of liquid slags are only slightly dependent upon structure. It is customary to model the density through the molar volume (V) where 1, 2, 3 denotes $\text{SiO}_2, \text{CaO}, \text{Al}_2\text{O}_3$ etc. and M= molecular weight of slag.

$$V = \sum (X_1 V_1) + (X_2 V_2) + (X_3 V_3) + (X_4 V_4) + \quad (30)$$

$$\rho = M / V \quad (31)$$

for a binary system eg CaO- SiO_2 we can determine the value of V for a specific oxide eg. SiO_2 from measured V (from ρ for slag) and the relation:

$$X_1 V_1 = V - X_2 V_2 \quad (32)$$

If V_1 is unaffected by structure it would have a constant value for all mole fractions; in practice it was found that V_1 increased as the SiO_2 content (ie X_1) increases. ($V_1 = 19.55 + 7.966 X_{\text{SiO}_2}$). Similar relations were also found for Al_2O_3 and P_2O_5 in silicate slags. Similar methods can be used to calculate the density of the solid slag at 298 K and values at higher temperatures can be derived by using the calculated thermal expansion data:

$$\rho_T = \rho_{298} / (1 + \alpha T)^3 \quad (33)$$

The densities of many of the components of the slag are similar and Keene [42] proposed a simple relation for calculating the densities of molten steelmaking slags with an uncertainty of ca. $\pm 5\%$.

$$\rho_{1673}(\text{kgm}^{-3}) = 2490 + 12 (\% \text{ FeO} + \% \text{ Fe}_2\text{O}_3 + \% \text{ MnO} + \% \text{ FeO}) \quad (34)$$

The transition at T_g of glass→scl results in a larger density- temperature gradient for temperatures $>T_g$.

Modelling densities off molten and solid slags

The densities of many molten slags can be determined to a reasonable accuracy ($\pm 2-3\%$) by the simple method outlined above (Equns 30 - 33). The available methods are summarised in Table 3. Various methods are used to account for the dependence on structure eg .via the excess free energy [41]etc.

Table 3: Details of models to calculate densities of alloys and slags

Reference	System	Details of Method	Uncertainty
Bottinga Weill [44]	Slags	$V = \sum X_i V_i + X_2 V_2 + X_3 V_3$ Values of V given Corrections to V values for compositions of Al_2O_3 , Na_2O , K_2O , CaO , MgO , FeO : Equations for β also corrected for chemical compositions of these oxides	2-3%
Mills Keene[42]	Slags	Method 1: ρ (kgm^{-3}) = 2460 + 18 (% FeO + % Fe_2O_3 + % MnO + % FeO) Method 2: $V = \sum X_i V_i + X_2 V_2 + X_3 V_3 + \dots$ at 1773K V ($10^{-6} m^3 mol^{-1}$) values for: CaO=20.7; FeO= 15.8; Fe_2O_3 = 38.4; MnO = 15.6; MgO= 16.1; Na_2O = 33; K_2O = 51.8; TiO_2 = 24; P_2O_5 = 65.7; SiO_2 = (19.55 + 7.97 X_{SiO_2}) Al_2O_3 = (28.3+ 32 $X_{Al_2O_3}$ -31.45 $X_{Al_2O_3}^2$) (dV/dT) = 0.01% K^{-1}	5% 2%
Robinson et al [40]	Slags	Use of thermodynamic software: Molar volumes stored for oxides and correction based on molar Gibbs energy of system	2%
Hayashi, Seetharaman [45]	Slags	$V / \sum X_i V_i = (K \Delta^{mix} H / R^* T)$ where is the relative integral enthalpy of mixing (determined with thermodynamic software) and K= constant	2%
Persson [41]	Slags	$V^M = \lambda H^M$. $\sum X_i V_m / R^* T$ where M and m indicate integral and partial molar volumes, λ is a constant and H^M is the integral enthalpy of mixing Values of ΔG^M , λ and interaction coefficients obtained from thermodynamic model	2-5%
Priven [46]	Glasses	Solids: $V = \sum X_i V_i + X_2 V_2 + X_3 V_3$ Values and range of applicability given. Special procedures for boro-silicates	

4.5 Viscosity (η) of slags

Viscosity is the ability to resist the movement of one layer of molecules over another when a stress is applied (via a rotating cylinder in most experiments). **It should be noted that the units of all viscosities cited here are for dPas.**

4.5.1 Factors affecting property: Viscosity is very structure dependent upon both structure and on temperature since increased temperature also tends to break down the structure. The Arrhenius equation (Equn 35) is widely used to express the temperature dependence of viscosity but the Weymann (or Frenkel) relation (Equn 36) and other equations have been used and can provide a slightly improved fit.

$$\eta = (A_A \cdot \exp B_A / T) \quad (35)$$

where A_A is constant dependent upon the slag structure and $B_A = E_\eta / R^*$ where E_η is the activation energy for viscous flow (which too is dependent upon structure) and R^* is the Gas constant.

$$\eta = (A_W \cdot T \cdot \exp B_W / T) \quad (36)$$

where A_W and B_W are similar to the A_A and B_A parameters in Equn 35 but will have different values .Some workers [47,29,30] have linked A and B (or A_W and B_W) via equations since both are related to structure.

For glassy slags (eg $Q > 3$) there is a rapid increase in viscosity on cooling (Figure 13a) as the slag moves from a liquid to a super-cooled liquid (scl) with the viscosity attaining a value of $10^{13.4}$ dPas at T_g . The temperature dependence in this scl range is usually expressed in the form of the Vogel-Fulcher- Tamman relation (Equn 37).which requires the knowledge of three constants A,B and T^0 .

$$\eta = A_V \exp (B_V / (T - T^0)) \quad (37)$$

4.5.2 Methods of measurement

The most popular method of measuring slag viscosities is the concentric cylinder method, which consists of centrally –aligned bob in a cylindrical crucible [43]. The method can be operated by measuring the torque when rotating either the bob or the crucible [43]; the rotating bob method tends to be more popular because of ease of operation. Rotation speed is determined by the viscosity and torque measured and it is usual to make measurements at least two different speeds to ensure the flow is Newtonian.

Falling sphere and capillary viscometers have been used for slags but tend to be difficult to operate at high temperatures because of the need for a large zone of uniform temperature. Oscillating viscometers have been used for measuring de-polymerised slag viscosities[43].

The uncertainty in the measurements for many slags is ca. $\pm 20\%$ because of changes in slag composition during the measurement and from systematic errors arising from end effects etc. The very best viscosity measurements are probably subject to an uncertainty of ca. $\pm 10\%$.

4.5.3 Modelling of slag viscosities

A number of models have been reported to estimate viscosity; they all account for the structure in some form and details of the method are given in Table 4. The cited uncertainties in estimated values for different slag systems are also given.

Table 4: Details of published models for the estimation of slag viscosities; Arr= Arrhenius relation; Wey= Weymann relation; Emp= Empirical relation; Syn= Synthetic slag; BF= Blast furnace slags; $\Delta\% = (\sum \delta_n \%) / N$ where $\delta\% = 100\{(\eta_{meas} - \eta_{calc}) / \eta_{meas}\}$ and $N =$ number of measurements.

Reference	Slag Type	T-Dependence	Details of model and comments	Slag	$\Delta\%$
Riboud et al [24]	Variou s	Wey	$A_W; B_W$ functions of 5 groups "CaO"+"SiO ₂ "+"Al ₂ O ₃ "+"CaF ₂ "+"Na ₂ O" Where X_{CaO} contains $X_{CaO} + X_{MgO} + X_{FeO} + X_{MnO}$ etc. $\ln A = -19.81 + 1.73 X_{CaO} + 3.58 X_{CaF_2} + 7.02 X_{Na_2O} - 35.76 X_{Al_2O_3}$ $B = 31140 - 23896 X_{CaO} - 46356 X_{CaF_2} - 39159 X_{Na_2O} - 68833 X_{Al_2O_3}$ Works well (30%) for variety of slags	Slag Mould flux	30
Urbain [47]	Variou s	Wey	$A_W; B_W$ functions of 3 groups " Glass formers: $X_G = X_{SiO_2} + X_{B_2O_3}$ Amphoterics $X_{Al} = X_{Al_2O_3} + X_{B_2O_3} + X_{Fe_2O_3}$ Modifiers: $X_M = X_{CaO} + X_{MgO} + X_{Na_2O} + 3 X_{CaF_2} + X_{FeO} + X_{MnO} + 2 X_{TiO_2} +$ $B_W = B_0 + B_1 X_G + B_2 X_G^2 + B_3 X_G^3$ and $Bi = \alpha I + bi\alpha + ci\alpha^2$ $\ln A_W = 0.2693 B_W + 11.6725$ Special B_W values for MnO, MgO	Variou s	25
Iida et al [48]	Many	Arr	η (Pas) = $A\eta_0 \exp(E/Bi)$ where η_0 is viscosity of hypothetical network-forming melt and Bi = basicity index $E = 11.11 - 3.65 \times 10^{-3} T$ and $a = 1.745 - 1.962 \times 10^{-3} T + 7 \times 10^{-7} T^2$ and $Bi = \sum(\alpha_i \%i)_B / \sum(\alpha_i \%i)_A$ where A = acid oxides and B = basic oxides or fluorides : $\eta = 1.8 \times 10^{-7} (M = i T^m)^{0.5} \exp(H_i / RT^m) / V_{jm}^{0.667} \exp(H_i / RT^m)$ where $H_i = 5.1 T^m$ and values of α given	Mould flux BF	25 19
Senior [49]	Coal	Wey	$A = a_0 + a_1 B + a_2 (NBO/T)$ where $a_0 = 2.816$ $a_1 = 0.4634$: $a_2 = 0.3534$ $(NBO/T) = X_{CaO} + X_{MgO} + X_{Na_2O} + X_{FeO} + X_{MnO} - X_{Al_2O_3} + X_{Fe_2O_3} / \{0.5(X_{SiO_2} + X_{TiO_2}) + X_{Al_2O_3} + X_{Fe_2O_3}\}$ Equations also given for low temperatures		
Mills et al [50]	Variou s	Arr	Optical basicity (Λ)- measure of depolymerisation Composition adjusted for Al ₂ O ₃ needed for charge balancing $\rightarrow \Lambda_{corr}$ $\ln A = -232.7 (\Lambda_{corr})^2 + 357.3 (\Lambda_{corr}) - 144.2$ $\ln (B/100) = -1.77 + (2.88/\Lambda_{corr})$ $\ln \eta$ (Pas) = $\ln A + \exp(B/T)$	Mould flux	34
Gupta et al [51]	Mould fluxes	Arr	3 groups "Acidic": $Y_X = (\%SiO_2 / 60) + \alpha (\%Al_2O_3 / 102)$ "Basic" $Y_O = (\%CaO / 56) + (\%MgO / 40) + (\%Na_2O / 63) + (\%FeO / 72)$ "Fluorides" $Y_F = (\%F / 19)$: $N_F = Y_F / (Y_X + Y_O + Y_F)$: $N_X = Y_X / (Y_X + Y_O + Y_F)$: $N_O = Y_O / (Y_X + Y_O + Y_F)$ Na^+ / Ca^{2+} affected η : Values of a_0 to a_5 given for 1573 and 1673 K $\eta = a_0 + a_1 (M^+ / M^{2+}) + a_2 N_X + a_3 N_X (M^+ / M^{2+}) + a_4 (M^+ / M^{2+})^2 + a_5 N_X^2$	Mould flux	35
Koyama et al [52]	Mould fluxes	Arr	$\ln A = -24.2 X_{Al_2O_3} - 6.1 X_{CaO} - 12.1 X_{MgO} - 19 X_{Na_2O} + 6.3 X_{CaF_2} - 4.816 B - 9259 X_{SiO_2} + 28319 X_{Al_2O_3} - 16564 X_{CaO} - 41365 X_{CaF_2} - 45510 X_{Li_2O} + 29012$	Mould flux	76
Kim et al [53]	Mould fluxes	Arr	$\ln A = -2.307 - 0.046 X_{SiO_2} - 0.07 X_{CaO} - 0.041 X_{MgO} - 0.185 X_{Al_2O_3} + 0.035 X_{CaF_2} - 0.095 X_{B_2O_3}$ $B = 6807 + 70.7 X_{SiO_2} + 32.58 X_{CaO} + 312.7 X_{Al_2O_3} - 34.8 X_{Na_2O} - 176.1 X_{CaF_2} - 167.4 X_{Li_2O} + 59.7 X_{B_2O_3}$ where X in mole %	Mould flux	45
Utigard et al.	Non-	Emp	$\log \eta$ (Pas) = $-0.49 - 5.1 (VR)^{0.5} + (-3660 + 12080 (VR)^{0.5}) / T$		

[54]	Ferrous		VR= A/B where A =SiO ₂ + 1.5 Cr ₂ O ₃ +1.2 ZrO ₂ +1..8 Al ₂ O ₃ B= 1.2 FeO +0.5(Fe ₂ O ₃ + PbO) + 0.7 (CaO +Cu ₂ O) +0.8 MgO + 2.3 (Na ₂ O +K ₂ O) + 1.6 CaF ₂ where in wt %		
Reddy [55]	Binary Boro-silicate	Emp	η (dPas) = 4.9 x10 ⁻⁹ N ₀₀ T ^{0.5} exp (E/RT) N ₀₀ calculated from atomic pair (thermodynamic)model E related to N ₀₀		
Du and Seetharaman [32, 33]	Syn	Arr	$\eta = hN_A \rho / M \exp (\Delta G_\eta / RT)$ where h= Planck constant, N _A = Avogadro No Structure accounted for - thermodynamics: $\Delta G^*_\eta = \Sigma \Delta G^*_\eta$ (oxides) + $\Delta G_\eta^{mix} + 3R^*T X_1X_2$ ΔG_η^{mix} for interactions of cations only Works well for synthetic slags ($\pm 15\%$)	Syn	<20
Ling Zhang et al[30,31]	Various	Wey	Structure as N _O ; N _O ; N _{O2} . calculated from cell model (thermodynamic) A _w and B _w as functions of - N _O ; N _{O2} . Molecular Dynamics calculations Works well (20%) several slags	Coal	22
Tanaka [56]	Syn	Arr	X _O ; X _O ; X _{O2} . calculated from thermodynamic cell model N _{MO} = a * (X _O + X _{O2}) where a* is a measure of free space available and n is the frequency of the step in MO-SiO ₂ system: a* values :Al ₂ O ₃ = 0.95; MgO =1.8; CaO=2.0 and FeO= 3.8 Multicomponent slags: E _η =E ₀ / (1+ Σ a* X _O) ^{0.5} where E ₀ = E _η for SiO ₂		
Kondratiev, Jak I[57]	Coal; Syn	Wey	Modified Urbain method for CaO +FeO+Al ₂ O ₃ + SiO ₂ system Modification 1: -ln A= mB+N; n=9.322 but m is composition dependent m= m ₁ X ₁ + m ₂ X ₂ + m ₃ X ₃ + m ₄ X ₄ + and values given for various m values Modification 2: Different B values given for FeO and CaO; constants given to calculate B values	Syn	25
Robinson [40]	Syn	Arr	Uses Thermodynamic software: data for binaries. Based on Du and Seetharaman model		
Nakamoto [22,23]	Syn		Neural network model based on experimental data	Syn	<22

4.6 - Electrical conductivity (κ) – Electrical resistivity(R)

Electrical conduction in molten slags occurs through the movement of ions when an electrical field is applied. Since anions are polymeric they tend to be large and do not move readily, so the electrical conductivity is usually associated with the movement of cations eg. Na⁺, Ca²⁺ etc. Electrical resistivity (R=1/ κ) is the measure of the resistance to ionic transport provided by the molten slag.

The specific electrical conductivity (κ) is the conductivity of a 1 metre cube of the sample and is given by the relation:

$$\kappa = F \sum cz u \quad (38)$$

where F= Faraday constant, c , z and u are the concentration, charge and mobility of the ionic species. The temperature dependence is usually represented by the Arrhenius equation:

$$\kappa = A_\kappa \exp (-B_\kappa / T) \quad (39)$$

where A_κ=constant ; B_κ = (E_κ/ R*), E_κ = Activation energy and R* =Gas constant =8.314 JK⁻¹mol⁻¹ and T in K

$$\ln \kappa = \ln A_\kappa - (B_\kappa / T) \quad (40)$$

similarly for resistance

$$\ln R = \ln A_R + (B_R / R^*T) \quad (41)$$

When a metallic electrode is submerged in a molten electrolyte there is a potential difference across the interface. One phase acquires a positive charge and the other a negative charge. The Helmholtz model assumes a layer of charge at the electrode surface to which ions of the opposite charge in the electrolyte are rigidly held (Figure 19 a) and is equivalent to a simple parallel plate capacitor. In the Stern model the charges are adsorbed on the electrode surface and are rigidly fixed there by the presence of an immobile

layer of oppositely charged ions in the melt (Figure 19b). The Stern model allows for the thermal motion of ions.

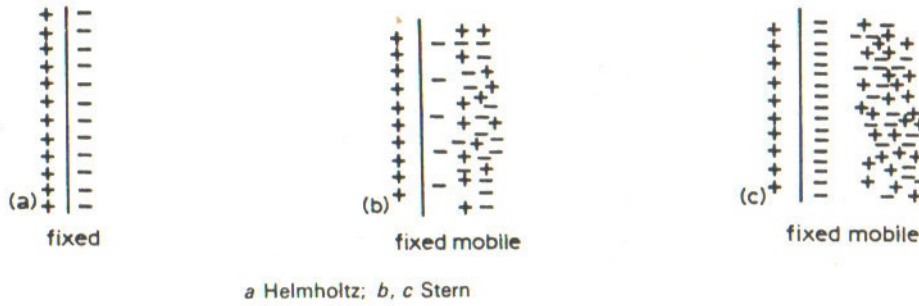


Figure 19: Schematic drawing of models of double layer (a) Helmholtz (b,c) Stern models

4.6.1 Factors affecting property-

Electrical resistivity (R) will increase as the size of the polymeric units increase. Thus R would be expected to increase as Q increases and (NBO/T) and optical basicity decrease. Since the addition of Al₂O₃ effectively increases polymerisation, R will be a function of Q^{corr}; (NBO/T)^{corr} and Λ^{corr}. The nature of the cations also affects the effects the electrical conductivity. The charge (z) on ions eg 2 for Ca²⁺. affects the resistance since a Ca²⁺ ion will bridge 2 chains whereas a Na⁺ will not (Figure 20), hence the resistance to the movement of ions will be greater in CaO-slugs than in Na₂O-slugs. However, there are other factors (i) there are twice as many Na⁺ cations to Ca²⁺ (for any given Q) -ie. twice the number of potential cations available for transport (ii) smaller cations will slip through the holes in the network more easily than bigger cations but this is offset by the fact that a smaller cation has higher polarisability. Zhang et al. reported that for M₂O –SiO₂ slags κ decreases as the cation radius (r) increases (κ ↓ as r ↑) whereas the situation is reversed for Mg, Ca, Sr, and Ba oxide- slags (κ ↑ as r ↑). It is considered that any cations engaged in charge-balancing duties are not available for movement (ie electrical conduction)

Zhang, Chou et al [58,59] plotted ln κ vs ln η (Fig 21) and found that for a given viscosity κ(M⁺) > κ(M²⁺). This was attributed to (i) the concentration of M⁺ ions is twice that of M²⁺ ions and (ii) increases in the resistance due to the *bridging* of two chains by one Ca²⁺ cf no bridging of networks by Na⁺ (see below)

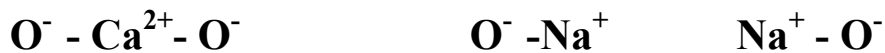
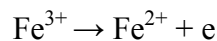


Figure 20: Schematic diagram showing (a) “bridging ” of two O⁻ in chains by Ca²⁺ and (b) absence of “bridging” with Na⁺ ions.

Transition metal oxides have more than one valence eg. Fe²⁺ and Fe³⁺. Consequently, there is the possibility that ionic conduction could occur by charge transfer between Fe²⁺ and Fe³⁺.



Similar reactions can occur with other transition metal oxides eg Cr³⁺ and Cr²⁺. At high concentrations of FeO_x etc there is the possibility of electronic transport which causes a significant increase in the total conductivity [98]. The electrical conductivity of slags containing FeO_x were determined as a function of pO₂ and κ was found to go through a maximum at ca. pO₂= 10⁻⁶atm [97]. An attempt was made to model the effect of oxidation state into a model of the electrical conductivity [97] according to Jahanshahi et al. [99]; this information was not available to me.

4.6.2 Size of cations

The size (r) of the cations affects the conductivity because small cations are more mobile than larger cations and can slip through the “holes” in the network. Zhang, Chou et al. [58,59] plotted data in Figure 21 for Ba²⁺, Sr²⁺, Ca²⁺, Mg²⁺, it can be seen that for a given viscosity the conductivity of Ca²⁺ and Mg²⁺ is

slightly greater than Ba^{2+} ; this may be due to the greater mobility of the smaller cation or may be due to greater resistance to “bridging of chains“ with bigger cations.

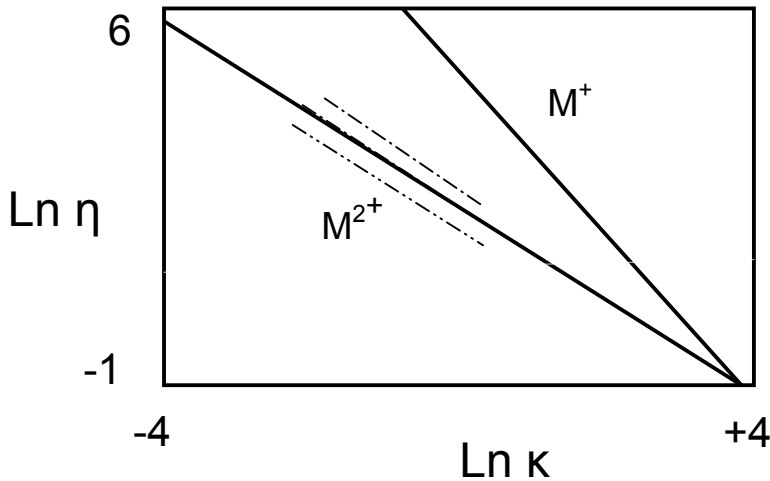


Figure 21: Schematic diagram representing plot of \ln viscosity (Pas) vs \ln conductivity ($\Omega^{-1}m^{-1}$) for divalent and monovalent ions.(after Chou) ; dash –dot line= Ca^{2+} dash-double dot line= Ba^{2+} [59]

4.6.3 Factors affecting measurements

Polarisation is the principal problem and arises from concentration gradients arising in the electrolyte and manifests as a back EMF opposing the normal ionic flow. The 4-wire method is used to minimise polarisation where 2 electrodes carry the current and the other 2 monitor the potential.

Frequency (f) has been reported to affect κ [43] ; some workers assume that the impedance of electrolyte region is a function of f^{-1} .

4.6.4 Measurement methods

The various methods are described in the Slag Atlas [43] and ,in general, it is preferable to have the two electrodes with similar areas (Figures 22 c and d). Methods can be divided into the various 2-electrode (Figure 22a,b, c) and 4-electrode methods (Figure 22d) with preference being given to the latter since it minimises problems associated with polarisation.

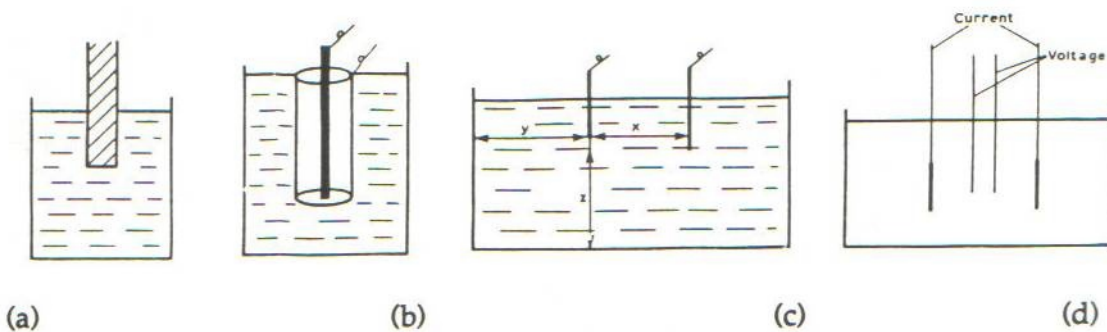


Figure 22: Cell arrangements for measuring electrical conductivities of molten slags (a) central electrode (b) ring-cell (c) 2-electrode cell (d) 4- electrode cell

4.6.5 Methods of estimating electrical conductivity

Until recently there were no models available to calculate the electrical conductivity (κ). Jiao and Themelis [96] obtained an empirical relation for $CaO+MgO+ MnO+SiO_2$ slags at 1773K: however, this equation is of limited use for the estimation of the electrical conductivity of industrial slags:

$$\kappa_{1773} = -3.34 + 6.41 X_{CaO} + 6.45 X_{MgO} + 8.06 X_{MnO} \tag{42}$$

However, Zhang and Chou [58,59] have recently reported two models to calculate the thermal conductivity of some silicate melts.

Method 1 Estimation of electrical conductivity using optical basicity

There are two factors affecting the electrical conductivity:

- (i) The structure of the network which restricts the movement of cations ($\kappa \downarrow$ as polymerisation \uparrow)
- (ii) The nature of the cations which affect (a) the viscosity *ie* structure (b) the size of the cations (since small cations can move easier through the network) (c) the charge on the cations since there are twice the number of Na^+ ions to Ca^{2+} ions available for conduction and (d) the polarisability of the cation which increases as the cation radius decreases.

Zhang and Chou [58] used the corrected optical basicity (Λ^{corr}) to cover these effects of structure and cation size. The model is described below.

$$\ln \kappa = \ln A_{\kappa} - (B_{\kappa}/R^* T) \tag{43}$$

$$B_{\kappa} = m(\Lambda^{\text{corr}}) + n \tag{44}$$

Experimental data were regressed to obtain best fit values for A_{κ} , m and n (eg respectively, 5054, 3.24×10^5 and $-2.768 \cdot 10^5$ for the CaO-MgO-Al₂O₃-SiO₂ system and 9462, 3.197×10^5 and -2.49×10^5 for the CaO-Al₂O₃-SiO₂ system). The results are shown in Figure 21 and it is possible to distinguish small deviations for individual cations (Ba to the left and Ca and Mg to the right of the curve). The mean uncertainty in the calculated values was <15%. The model could be applied to slags whose composition lay within the range $\Lambda^{\text{corr}}=0.58-0.67$.

Method 2 Relation between electrical resistivity and viscosity

Zhang and Chou [59] reported that the electrical conductivity could be expressed as a function of the viscosity. They found that for the MO-systems $\ln \eta = 0.15-1.1 \ln \kappa$ and for M₂O-SiO₂ systems, $\ln \eta = 4.02-2.87 \ln \kappa$. These workers also plotted $\ln \kappa$ as a function of \ln viscosity (Figure 23) and found a reasonably linear relation with some scatter.

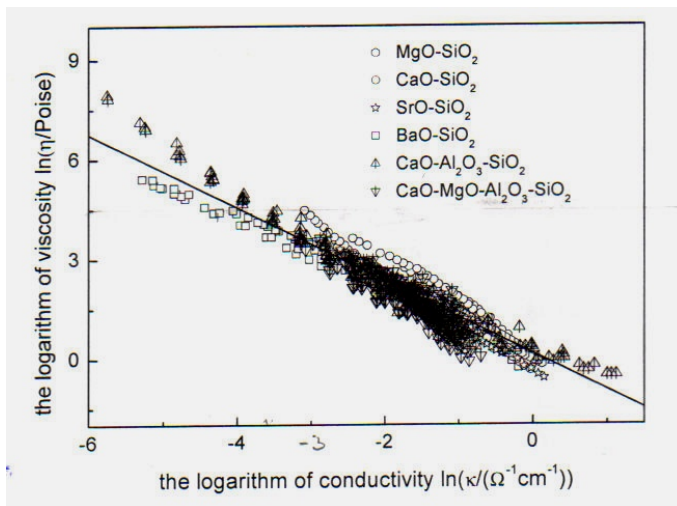


Figure 23: *ln* electrical conductivity as a function of *ln* viscosity [59].

Thus models for the estimation of electrical conductivities are in their infancy

4.7 Surface tension (γ)

4.7.1 Factors affecting property: Surface tension is not a bulk property. *Surface-active components* such as S or O in molten metals have a low surface tension compared with the metal and consequently, tend to occupy the surface layer in much higher concentrations (ca 100x) than the exist in the bulk.

Consequently, surface tension and its temperature dependence ($d\gamma/dT$) are extremely sensitive to S or O concentrations (Figure 23a); 50ppm S causes a decrease of 25% in surface tension and a negative ($d\gamma/dT$)

to go to a positive value. In slags there is not such a wide difference between the surface tensions of the surface-active components (eg. B_2O_3 and CaF_2 and SiO_2) and those of the other components (eg. CaO see Table 2) in the slag as there is with O or S in metals. Surface tensions of slags tend not to be very structure- dependent but since $\gamma_{SiO_2} < \gamma_{CaO}$ the surface tension tends to (i) decrease with increasing Q value and (ii) give positive ($d\gamma/dT$) values at higher SiO_2 (or Q) values (ie similar to High S (>50ppm)steels Fig 23 b). The surface tension of the slag is dependent upon (i) the concentration of the surface active components and (ii) the chemical activity of the surface active component which determines the surface active concentration in the surface layer. Consequently, models of surface tension tend to be based on the thermodynamics of the slag system.

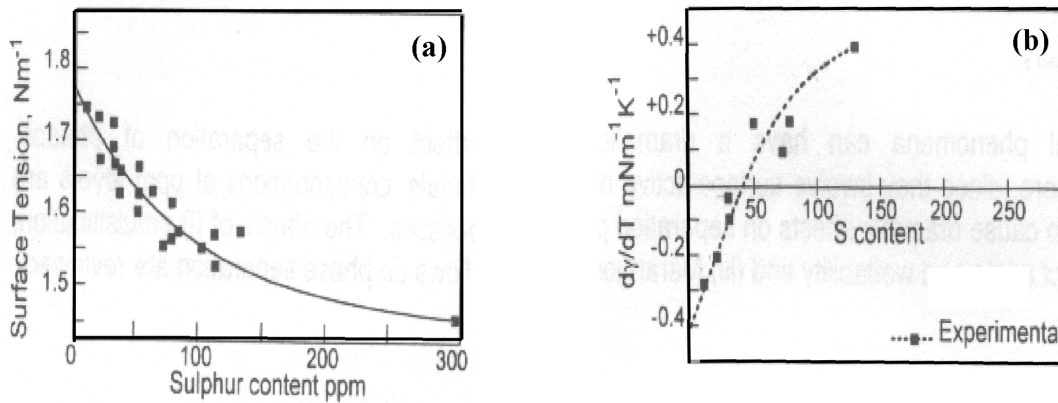


Figure 24: The effect of S concentrations on the (a) surface tension and (b) temperature coefficient ($d\gamma/dT$) of steels containing S

Table 2: Surface tensions (mNm^{-1}) of pure slag components at 1773K

	SiO ₂	CaO	BaO	SrO	MgO	Al ₂ O ₃	MgO	FeO	NiO	MnO	CrO	Na ₂ O	K ₂ O	TiO ₂	ZrO ₂	Cr ₂ O ₃	Fe ₂ O ₃	CaF ₂	B ₂ O ₃
γ	260	625	560	600	635	655	635	645	645	645	360	295	160	360	400	800	300	290	110

4.7.2 Measurement measurements

The principal methods used to measure surface tensions of slags [43,37] are (i) the sessile drop (SD) and pendent drop (PD) methods (ii) the maximum bubble pressure (MBP) method (iii) cylinder detachment method but newer methods like draining crucible and SLLS method may prove useful in the future. The accuracy of the SD and PD values have improved with the introduction of software to derive the parameters giving the “best fit” with the image of the experimental sessile or pendent drop. Surface tensions of many slags fall in the range 400- 500 mNm^{-1} . Typical experimental uncertainties are *ca.* $\pm 5\%$.

4.7.3 Methods of estimating surface tension

Tanaka et al [60,61] have applied their model for alloys to the calculation of the surface tension of slags and molten salts using commercial thermodynamic software to calculate $G^{XS,B}$ where the subscripts B and S refer to the bulk and surface, respectively. It was found that it was necessary to allow for the fact that the ionic distances in the surface differ from those in the bulk in order to maintain electrical neutrality. This was taken into account using the parameter, ξ , which was been applied to ternary systems but would be difficult to apply to multi-component systems.

$$(G^{XS}_S / G^{XS}_B) = (Z^S / Z^B) / \xi^4 = 0.94 / \xi^4 \quad (45)$$

with ξ having a value of 0.97.

Nakamoto, Tanaka et al [84,85] also reported a model based on the anionic and cationic radii and Butler equation which makes use of the molar volume of the slag components. The system was found to work successfully for a large number of ternary systems (including surfactants like CaF₂ and B₂O₃) but would be cumbersome when applied to quaternary and higher systems.

Other models have been reported for the calculation of the surface tension of slags [62-65]. The model due to Zhang et al. [65] makes use of the excess surface tension ($\gamma^{xs} = \gamma_{meas} - \sum X_i \gamma_i$) and derives constants to express (γ^{xs}) as a function of composition; good agreement was found for the calculated results with measured values.

Nakamoto et al [78] have developed a model based on the neural network approach. This approach is best applied to certain slag families or slag systems but would be less useful when applied to all slags. Estimated values were found to be within $\pm 4\%$ of the measured values.

Surface tensions and the trends in surface tension can be calculated using a partial molar approach. (Equation 45) and shown in Figure 25 [86]. The model divides slag components into two classes (i) oxides with higher surface tension values where $X_2 \gamma_2$ tends to be similar to that shown in Figure 25a and (ii) components with lower γ values (surfactants B₂O₃, CaF₂, Na₂O, K₂O, Fe₂O₃ and Cr₂O₃) where $X_2 \gamma_2$ is similar to that shown in Figures 25b and c.

$$\gamma = \sum X_i \gamma_i + X_2 \gamma_2 + X_3 \gamma_3 + \dots \quad (46)$$

These surface active components cause a rapid decrease in surface tension and in these cases $X_2 \gamma_2$ and can be represented by two curves determined by a critical point N (i) for $X_2 < N$ as a polynomial by $X_2 \gamma_2 = a + bX + cX^2$ and (ii) $X_2 > N$ by $X_2 \gamma_2 = a' + b'X$ (which are shown by the dashed line in Figure 25b). The biggest problem is the inability of the model to deal with two surface-active components simultaneously (eg. CaF₂ and B₂O₃) and the model tends to exaggerate the decrease in γ in these cases. The method has the advantage that it can easily be applied to multi-component industrial slags but uncertainties in the estimated values are ca. $\pm 10\%$.

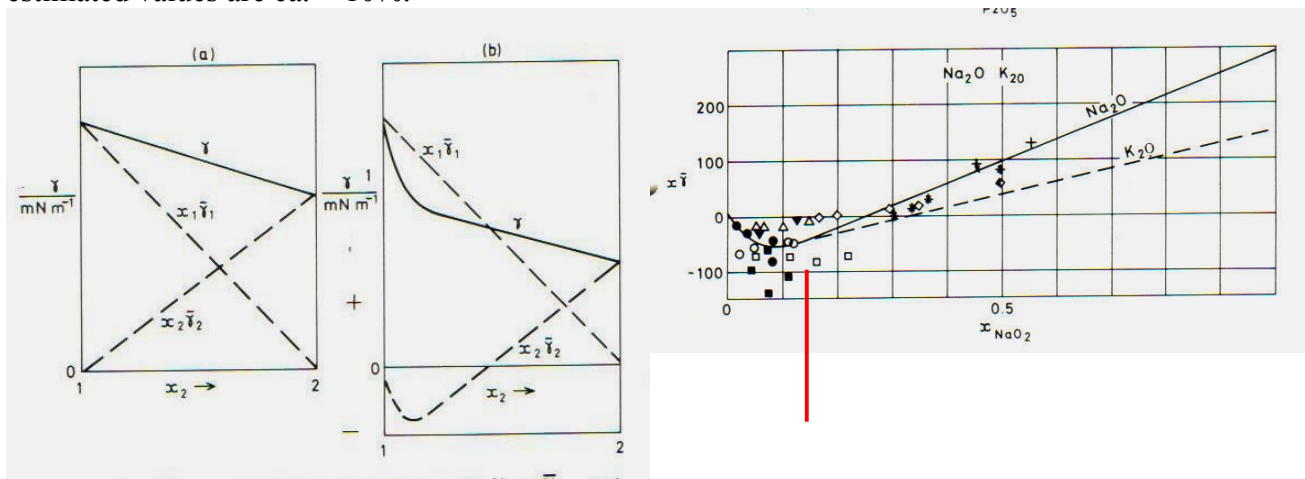


Figure 25: Composition dependence of γ and $x_i \gamma_i$ for binary slags with (a) non-surface-active constituents and (b) one surface active constituent (2) and (c) $X_2 \gamma_2$ as function of X_2 for Na₂O- and K₂O- SiO₂ slags with N value shown as vertical line.

Interfacial tension (γ_{MS})

Interfacial tensions can be calculated using the following relation

$$\gamma_{ms} = \gamma_m + \gamma_s + 2 \phi (\gamma_M \cdot \gamma_S)^{0.5} \quad (47)$$

where ϕ is an interaction coefficient. The parameter ϕ was found to have a value of 0.5 for slags free of FeO but increased with FeO additions [65]. Tanaka [15] proposed the following equation

$$\phi = 0.5 + 0.3X_{\text{FeO}} \quad (48)$$

Qiao et al. [66] have outlined a model for estimating the interfacial tension using the excess interfacial tension ($\gamma_{\text{MS}}^{\text{XS}}$) and considering the components of a binary alloy separately with regard to the slag. Values were derived for coefficients by fitting experimental data.

It should be noted that the surface tensions of metals tend to have surface tensions which are 3 to 4 x that for the slag (typically *ca.* 450mNm⁻¹) so the largest factor in Equn 47 is γ_{m} ; it follows that γ_{ms} is very dependent upon the soluble O and S contents of the metal (Figure 24).

4.8- Thermal conductivity –

4.8.1 Factors affecting thermal conductivity: The thermal conductivity of slags [68-76] involves the movement of phonons and this is usually referred to as *phonon conduction*. Consequently, the thermal conductivity (k) is very dependent on structure. The thermal conductivity of molten slags *increases* with *increasing* SiO₂ content in the slag (*ie.* the direct opposite of electrical conductivity). This is best viewed through the thermal resistance (1/k); the resistance to phonon transport is much smaller when passing along the chain than the resistance of moving phonons from chain to chain. Thus the more the slag is polymerised (*ie.* as Q increases or NBO/T decreases) the higher the thermal conductivity (Figure 26). It follows that because of this dependence on structure:

- the thermal conductivity is a function of the viscosity (see Figure 26a due to Hayashi et al.[68])
- the temperature dependence of k is best represented by similar functions to those for viscosity *ie.* Vogel-Fulcher relation for (T_g to T_{liq}) and the Arrhenius equation for T>T_{liq})

The thermal conductivity data also show that the cations affect the thermal conductivity values for alkali slags M₂O- SiO₂ the following hierarchy were observed $k_{\text{Li}} > k_{\text{Na}} > k_{\text{K}}$ (Hayashi et al.[68]) similar deviations were seen with the viscosity (B_A and ln A_A in hierarchy K>Na>Li). It is difficult to attribute the effect of these cations on (i) their effect on viscosity or (ii) mobility effects on heat transfer for individual cations.

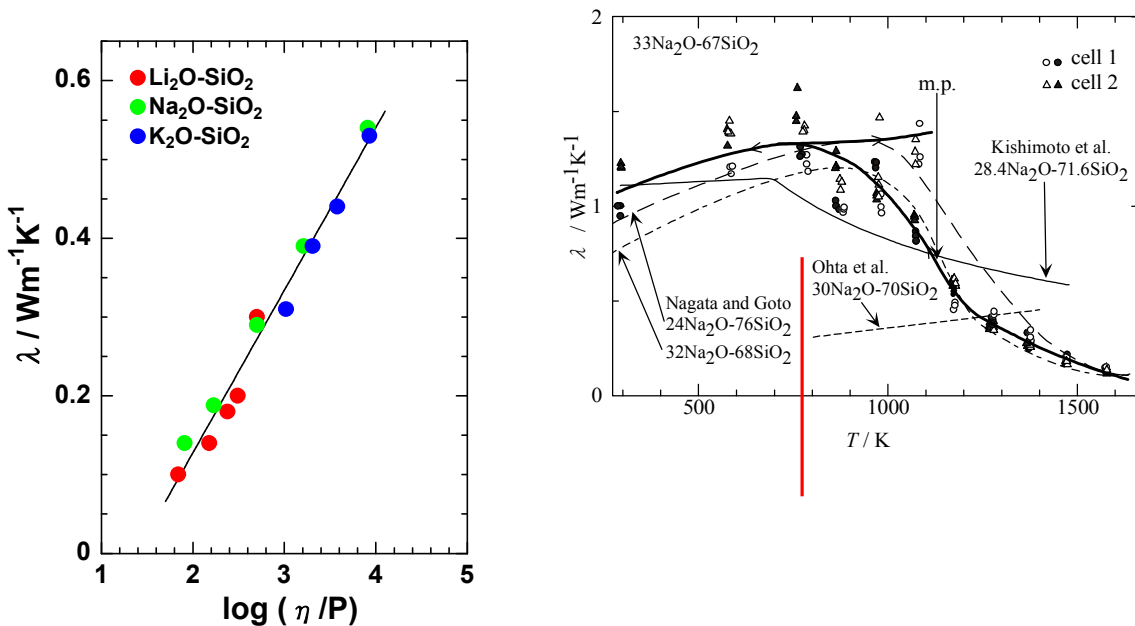


Figure 26: Diagrams showing (a) thermal conductivities of alkali silicates as a function of log viscosity and (b) Thermal conductivity of 0.33 Na₂O- 0.67SiO₂ as a function of temperature (after Hayashi [68])(Note T_g coincides with maximum conductivity and T_{liq}=mp)

There are two problems with measuring thermal conductivities of slags and glasses (i) eradicating convection for measurements on liquids and (ii) determining the amount of radiation conductivity; these are described in more detail below.

4.8.2 Convection contributions

The measured thermal conductivity for a liquid slag (k_{meas}) contains contributions from phonon conductivity (k_{meas}) and from convection (k_{conv})

$$k_{\text{meas}} = k_{\text{cond}} + k_{\text{conv}} \quad (49)$$

These contributions from convection can be large and so it is difficult to determine the true thermal conductivity of the molten slag but k_{conv} decreases as the viscosity of the slag increases. The following methods have been used to minimize k_{conv} :

- Using transient techniques (as opposed to steady state methods) where the duration of the experiment is too short (ca 1s) for convection to be initiated.
- Keeping the top of the sample hotter than the bottom
- Carrying out measurements in micro-gravity (space)
- Using magnetic fields to suppress the movement (mostly used on metals).
- It is claimed that measurements of thermal effusivity ($e=(kC_p\rho)^{0.5}$ = the ability to exchange thermal energy with its surroundings) are free of convective contributions.

4.8.3 Radiation conductivity (k_R)

In the 1960's it was noted that the apparent thermal conductivity (k_{app}) of solid glasses increased with increasing sample depth (Figure 27) until a constant value was attained when the depth exceeded a critical value (denoted as "*optically thick*") [77]. If a pulse of energy falls on the surface, the temperature of the surface layer increases and this layer is at a higher temperature than the layer 2 below it and so it radiates to layer 2. Now $T_{\text{layer 2}} > T_{\text{layer 3}}$ and emits to layer 3 and the process is repeated through the entire sample. Thus radiation conductivity consists of absorption of energy and re-emission of each layer through the sample (Figure 28). The sample becomes *optically thick* when $\alpha^* d > 3$ where α^* = absorption coefficient of the glass and d = thickness or depth of the sample. For optically thick samples k_R can be calculated from following equation where n = refractive index and σ = Stefan- Boltzmann constant and T is in K.

$$k_R = 16 \sigma n^2 T^3 / 3 \alpha^* \quad (50)$$

It can be seen that k_R is proportional to T^3 and hence increases dramatically at high temperatures. For molten glass 90% of the apparent thermal conductivity comes from k_R . In practice, the magnitude of k_R is reduced by:

- (i) transitional metal oxides (eg. FeO, NiO and Cr₂O₃) which cause a dramatic increase in α^* (eg. for FeO, $\alpha^*(\text{m}^{-1}) = 1100\% \text{FeO}$) and thereby reduce k_R .
- (ii) scattering of radiation (ie. k_R) by crystallites, grain boundaries etc in solid slag samples; in crystalline solids most of the radiated energy is scattered back to the source.

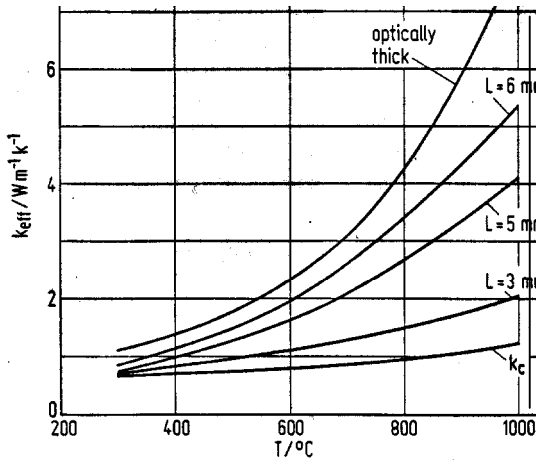


Figure 27: Apparent thermal conductivity as a function of sample thickness

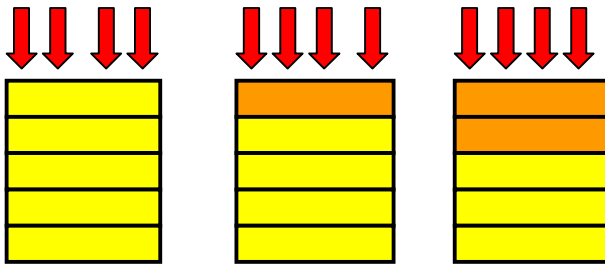


Figure 28: Schematic diagram showing the mechanism responsible for radiation conductivity

4.8.4 Measurement methods

There are two *transient* methods available for measuring the thermal conductivity of semi-transparent materials like slags and glasses viz. the laser pulse (LP) and the transient hot wire method (THW). The *transient hot wire* (THW) method (Figure 29a) consists of a thin Pt wire which acts as both a heating element and a temperature sensor (through a known Resistance-T relation). A current is passed through the wire for a short period of time (ca 1s) and the resistance (R) of the wire (which is a measure of the temperature) is monitored continuously and R is plotted as a function of \ln time (t). The plot shows 3 regions (i) an initial unstable region (ii) a stable region where the slope of the plot = $1/k$ and (iii) a region where convection kicks in and causes a drop in resistivity due to the cooling of the wire (ie. enhanced conductivity due to convection). Thus it is possible to detect the onset of convection (curvature at left hand side of T-t curve) with this method.

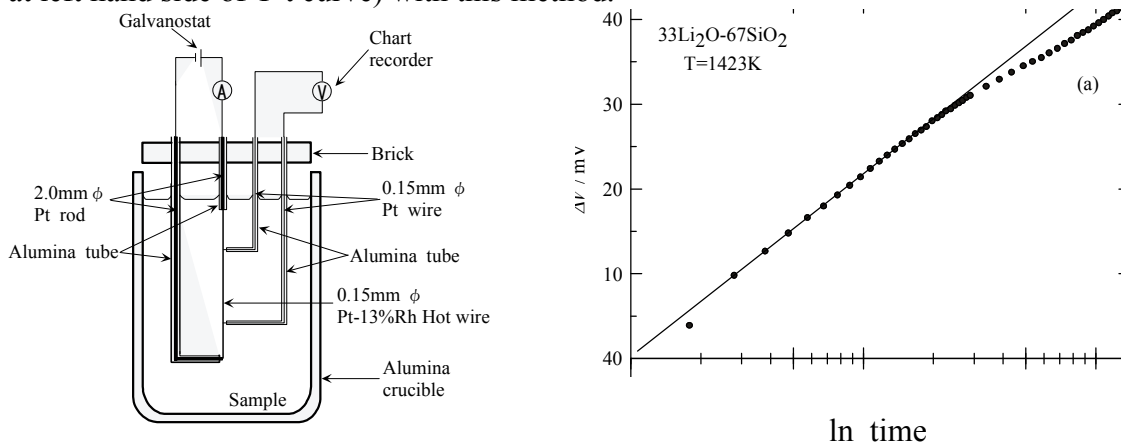


Figure 29: Schematic drawings showing (a) the transient hot wire method and (b) a typical output for slags.

In the Laser Pulse (LP) method (when applied to slags and glasses) a short pulse of energy is focused uniformly over a platinum disc located on the upper surface of the sample (ca 10mm diam x 3mm)

(Figure 30b) and the temperature of this disc is monitored continuously; the thermal diffusivity (a) can be calculated from the T_{disc} -time relation. Then the thermal conductivity is calculated via $k = a C_p \rho$

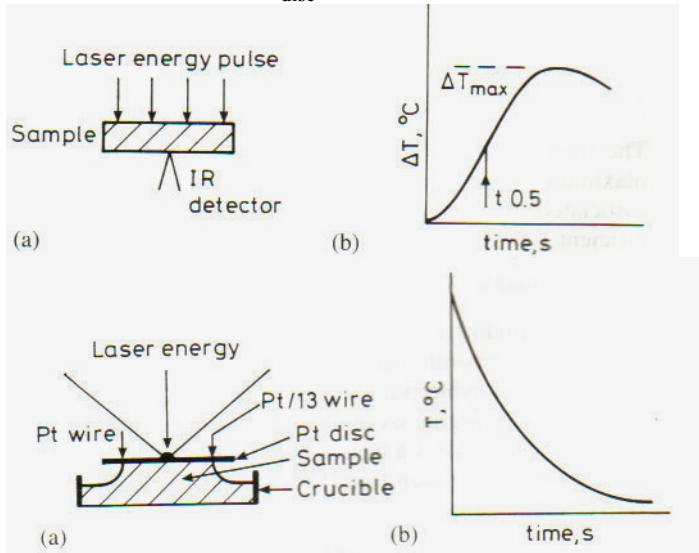


Figure 30: Schematic drawing of laser pulse method in (a) conventional manner (b) used following the attenuation of a Pt disc on the slag surface on left-hand side and T - t responses on right hand side.

4.8.5 Problems with measurements on slags and glasses

1. Measurements carried out with the THW and LP methods for the same slag composition indicate that $k_{\text{THW}} < k_{\text{LP}}$. This is thought to be due to a larger k_R contribution for the LP measurements due to the (surface area of disc) \gg (surface area of wire). Thus values measured contain an unknown contribution from k_R for both solid and liquid samples. However, this should not be the case for crystalline slag samples since most of k_R is reflected back to the source.
2. The measured values may not represent the samples in the industrial process eg. the liquid layer in the CC process is ca. 0.1mm thick and will be *optically thin* but the measurements in the laboratory are for *optically thick* conditions
3. It is very difficult to determine k_R for *optically thin* conditions.
4. Values are needed for optical properties (absorption coefficient and refractive index) are needed to calculate the magnitude of k_R for optically thick conditions

4.8.6 Thermal conductivity of crystalline slags

Nishioka et al [76] measured the thermal conductivity of $\text{CaO} + \text{Al}_2\text{O}_3 + \text{SiO}_2$ slags in both the glassy and crystalline state. As mentioned above it was found that $k_{\text{cryst}} = (1.5 \text{ to } 2.5) k_{\text{glass}}$ due to the increased packing densities. As can be seen from Figure 31 the temperature coefficient (dk/dT) was virtually independent of temperature over the range covered.

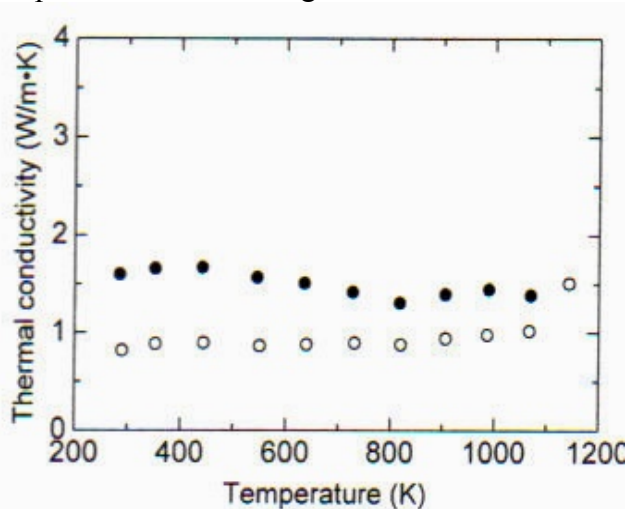


Figure 31: Thermal conductivity of glassy (O) and crystalline (●) slags as a function of temperature.

4.8.7 Modelling thermal conductivities of slags

The main problem with modelling thermal conductivities of slags is the accuracy of the measured data because of the problems (described above) associated with determining the magnitude of contributions from radiation conductivity and convection.

It has been reported that the thermal conductivity (k) increases as the SiO_2 content or the polymerisation (Q) in the slag increases or (NBO/T) decreases. This behaviour is consistent with good conduction along the covalently- bonded Si^{4+} chain and poor conductivity between chains.

For the solid phase the lattice (phonon) thermal conductivity for the crystalline phase is ca 2x larger than that for the glassy or amorphous phase (due to increased packing density). However, this enhanced heat transfer in crystalline slags is more than offset by the decrease in radiation conductivity (k_R) due to the scattering of the radiation by the crystallites. Thus k_{app} for glassy material is greater k_{app} of crystalline material ie. $q_{\text{cryst}} < q_{\text{glass}}$ where q =heat flux density.

Thus for glassy and liquid slags the heat transfer process is complex depends upon the sample thickness and it is important that experiments should provide a reasonable reproduction of the industrial situation Estimation in the case of glassy slags needs data for the various optical properties such as the absorption coefficient, refractive index etc.

It was decided to only use THW[68-75] data because of the difficulties of eradicating k_R effects from LP data when analysing thermal conductivity data. Thermal conductivity data show a reasonable amount of scatter and because of the relation between k and η it was decided to draw the $\ln k^m - Q$ in a similar way to that of $\ln \eta^m - Q$ curve (Figures 32 a and b); unfortunately, there are no data for $Q < 2$ which would have helped in the extrapolation of the curve.

The plots of $\ln k_{Tg} - Q$ and $\ln k_{298} - Q$ (Figure 33) show more scatter than the $\ln k^m - Q$ plot (Figure 32) but curves have been drawn to mirror the $\ln k^m - Q$; it was noted that the thermal conductivity of slags containing Li_2O were significantly higher than those for other slags and the curves in Figure 33 were drawn to reflect this. This suggests that the cations do have an effect on the thermal conductivity. The following equations were derived from the plots shown in Figures 32a and 33.

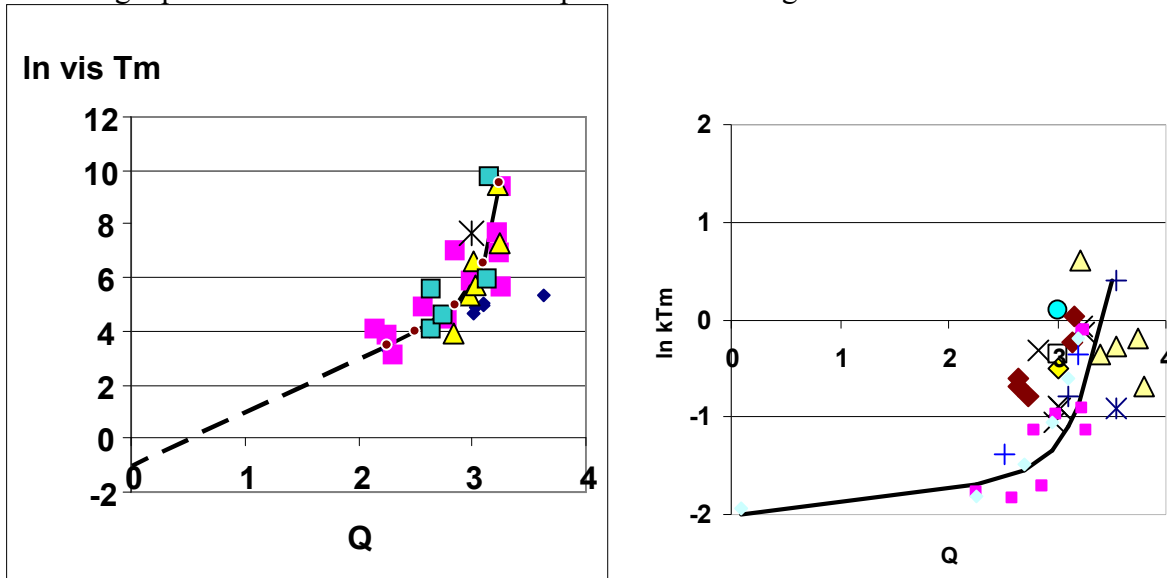


Figure 32: (a) $\ln \eta^m$ and (b) $\ln \eta^m$ as functions of Q : dashed line=extrapolation using data in [12]

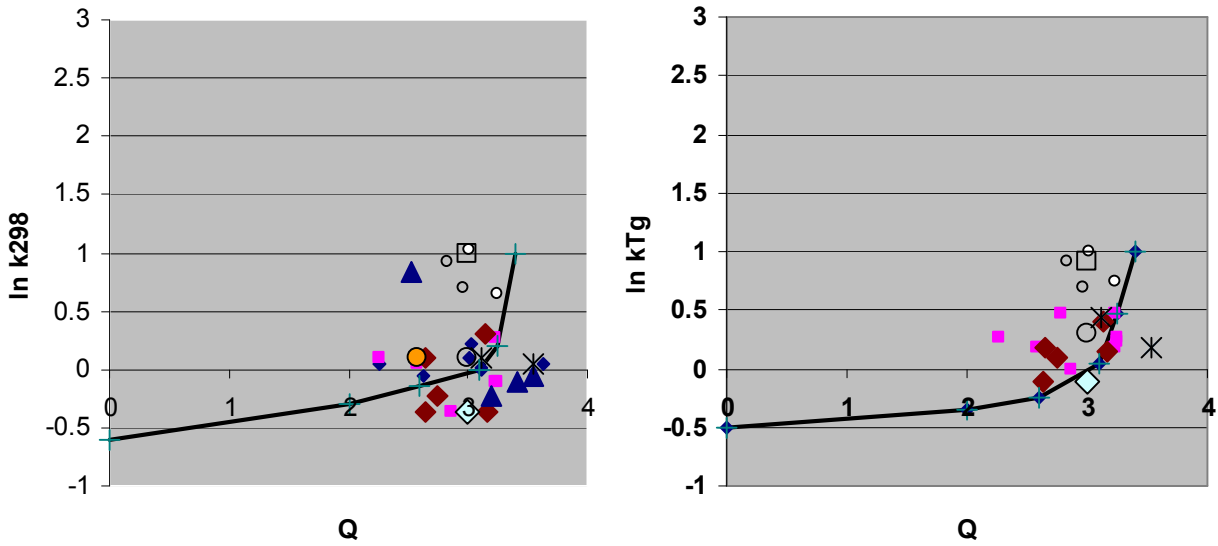


Figure 33: Values of (a) $\ln k_{298}$ and (b) $\ln k_{T_g}$ as functions of Q ; $o, \square = \text{Li}_2\text{O}$ -silicate slags.

Solid, 298K: $\ln k_{298} = -0.424 + 0.00002 \exp(Q / 0.299) + 3.2 X_{\text{Li}_2\text{O}}$ (51)

Solid: T_g $\ln k_{T_g} = -0.435 + 0.00005 \exp(Q / 0.332) + 3.0 X_{\text{Li}_2\text{O}}$ (52)

Liquid: T^{liq} $\ln k^m = -1.914 + 0.00037 \exp(Q/0.402)$ (53)

The thermal conductivity data were then used to explore the relation between viscosity and thermal conductivity for liquid slags (shown in Figure 34). The plot due to Hayashi et al [68] is for k vs $\ln \eta$ at various temperatures (Figure 34 a) whereas the other plot is for $\ln k^m$ vs $\ln \eta^m$ which yielded the following equation where k^m is in ($\text{Wm}^{-1}\text{K}^{-1}$) and η^m in dPas:

$$\ln k^m = -3.43 + 0.4 \ln \eta^m \quad (54)$$

The scatter in the data may be due to the uncertainties in T_{liq} which could lead to significant differences in η^m and k^m .

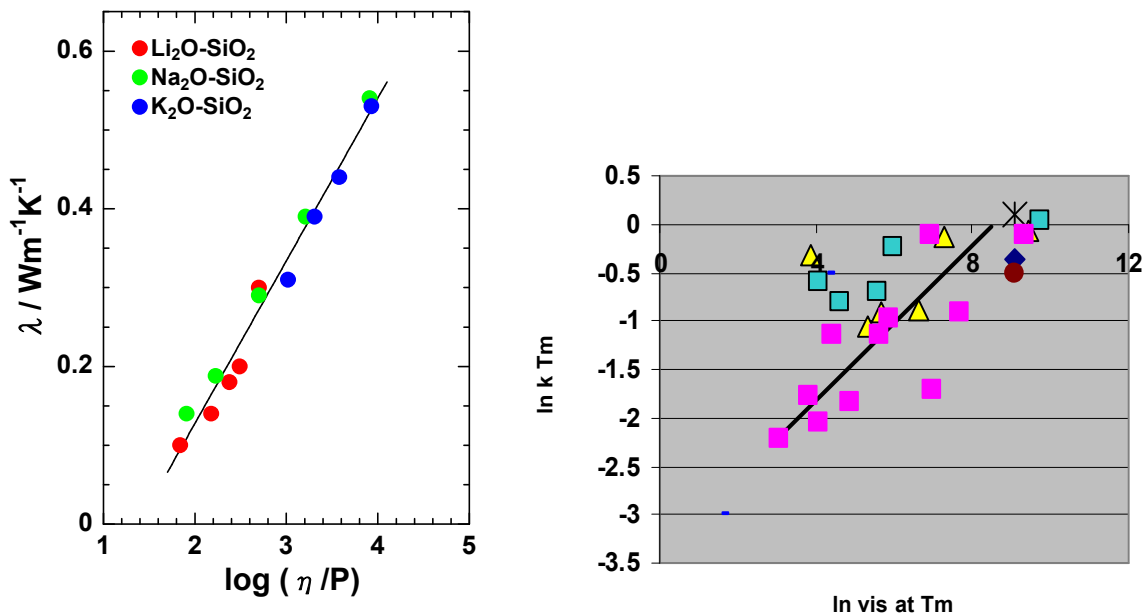


Figure 34: Thermal conductivity as a function of viscosity (a) k^m versus $\ln \eta$ [68] and (b) $\ln k^m$ vs $\ln \eta^m$

5. The model

Always work with a copy of the program- the master copy can get corrupted.

Start on the *Composition worksheet* all input data are fed into this worksheet

5.1 Composition worksheet

- It is necessary to insert (i) composition of slag in weight % and (ii) the liquidus temperature, T_{liq} or T^m and (iii) the selected temperatures which will be affected by the T_{liq} and T_g values
 - Insert slag composition into column C placing 0% where there is no content for a particular component and
 - note F is cited as F% and is subsequently converted by the model to X_{CaF_2}
 - a blank cell is provided (B 23) for other oxides but you will need to insert Molecular weight of oxides into cell H23 and various other cells in order to calculate the various properties.
 - Insert T_{liq} into cell B45 on this worksheet – **this must be done. It will appear automatically on other worksheets**
 - If you know the value of the glass transition temperature for glassy slags insert it in cell B –if you choose to let the model to calculate a value for T_g leave 0 in cell B30 and the calculated value (cell C30) will appear in the temperatures at cell 38.
 - Insert the selected temperatures (a) for glassy slags in cells B32 to B37 and B40 to B44 and for the liquid in cells B48 to B53. **Caution do not insert T_g and T_{liq} into column B this will be done automatically- if you do mistakenly insert a value it will corrupt this function.**
 - Insert the temperatures for the crystalline solid phase (no T_g involved) into column E cells 32 to 44- T_{liq} will appear automatically in E45
- The software
 - sums the slag composition and corrects the input values so that they total 100.0% (column D)
 - then allows for any pick-up during the process (this is principally aimed at CC fluxes)
 - the F% is then converted first to $\%CaF_2$ - this involves deducting $(56/38)*F\%$ from the CaO % in cell
 - the slag composition is then converted to **mole fractions (given in column J)** and note the mean Molecular weight is given in cell H24- also that values of 1000 are used in cells H23 to prevent calculations involving 0/0.
 - Values for (NBO/T) etc are calculated and are displayed in cell N4 and Q is given in cell O4 and the corrected opt basicity is given in cell S4

5.2 Collected Worksheet

All the calculated values are reported on this worksheet. **No input data are needed on this worksheet.**

Solid slag properties are reported in cells 5 to 19 with (i) glassy phase values between A and O and crystalline phase results between R and Z.

The calculated (approximate) value of T_g can be calculated by the following equation: In general, the estimated values will be within 50K of the true value but in some cases differences of 100 K could occur.

$$T_g(K)=1028-26X_{SiO_2}+189.5X_{CaO}-95.626X_{Al_2O_3}-996X_{Na_2O}-850X_{Li_2O}+598X_{K_2O}-59760X_{MgO}+7034X_{CaF_2}-6366X_{MnO}+3608X_{FeO} \quad (55)$$

Note the values of the constants for MgO, MnO and FeO were based on low concentrations and are unrealistic and thus should not be used when the mole fractions exceed >0.02

5.3 C_p and Enthalpy Worksheet

No data should be inputted into this worksheet. The software performs calculations of C_p and enthalpy ($H_T - H_{298}$) for *crystalline* slags, *glassy* (ie. *amorphous* slags) and *liquid* slags. The database is given in cells E27-E49-Q47-Q27. It should be noted that these values are given in cal mol^{-1} and so should the data be modified or added to the inserted data should be converted to $\text{cal mol}^{-1} = 4.184 \text{Jmol}^{-1}$.

5.3.1 Crystalline slag

The method has been described above in Section 4.2. The C_p are calculated for various temperatures in columns N and O for units $\text{JK}^{-1}\text{kg}^{-1}$ and $\text{JK}^{-1}\text{mol}^{-1}$, respectively, and ($H_T - H_{298}$) values for units of kJkg^{-1} and kJmol^{-1} , respectively, in columns Q and R.. The entropy of fusion (ΔS^{fus}) was calculated from the partial molar entropies (Equation 23) and then $\Delta H^{\text{fus}} = T_{\text{liq}} * (\Delta S^{\text{fus}})$ where T_{liq} is the inserted liquidus temperature.

5.3.2 Liquid slag

The C_p for the liquid is calculated from the partial molar values of the individual slags ($\sum X_i C_{pi}$) see Equation 19 and C_p for the liquid is assumed to be independent of temperature. Values of C_p for the liquid are given for units of $\text{JK}^{-1}\text{kg}^{-1}$ and $\text{JK}^{-1}\text{mol}^{-1}$, respectively, in columns N 20-25 and O 20-25. and ($H_T - H_{298}$) values for units of kJkg^{-1} and kJmol^{-1} , respectively, in columns Q 20-25 and R 20-25.

5.3.2 Glassy, amorphous slags

Glassy slags show a step-wise increase of $0.3 \text{ kJ K}^{-1}\text{kg}^{-1}$ at T_g . The basis of the calculation is that ($H_T - H_{298}$) value at T_{liq} ($=T^m$) for the liquid phase will be identical to that at obtained with the crystalline phase. We assume that for the range ($T^m - T_g$) that $C_p = a' + b'T$ and it can be shown that

$$b' = 2 * \{ (\Delta / (T_m - T_g)) - a' \} / (T^m + T_g) \quad (56)$$

where $\Delta = (H_{T_m} - H_{298})_{\text{cryst}} - (H_{T_g} - H_{298})_{\text{glass}}$ and $a' = C_{p\text{scl } T_g}$. The values of b' were determined (cell B 14) and C_p and ($H_T - H_{T_g}$) calculated for the $T_g - T_{\text{liq}}$ range.

- T_g will appear in E15 and E16 and other temperatures will appear between cells E8 and E14 and cells E16 and E19 and for the liquid in cells E22 to E25
- $T_{\text{liq}} = T^m$ will appear in E20
- The step-wise increase of $0.3 \text{ kJ K}^{-1}\text{kg}^{-1}$ which occurs at T_g (when $C_p = 1.1 \text{ kJ K}^{-1}\text{kg}^{-1}$) will be shown in E16
- The model assumes a linear increase in C_p between T_g and T_{liq} .
- All of the estimated values should lie within $\pm 5\%$ of measured data and for many cases will lie within $\pm 2\%$.

5.3.3 Crystalline slags

Values of C_p and ($H_T - H_{298}$) are calculated using Equations 19 to 24.

5.4 Density Worksheet

No data should be inputted into this worksheet

5.4.1 Liquid slags

The densities of liquid slags are calculated using the method outlined in Section 4.4 Table 3(–second model [42], which is essentially one of partial molar volumes but with molar volumes of SiO_2 and Al_2O_3 represented by equations. The densities are calculated for a reference temperature of 1773K and then adjusted for other temperatures by applying a temperature coefficient of $-0.01\% \text{ K}^{-1}$.

5.4.2 Solid slags

Crystalline slags: Slags with crystalline phases have a higher density than glassy, amorphous slags and will show a marked change in density at T_{liq} . The slag densities are estimated at 298 K by using a very

similar method to that adopted for the liquid phase. The values at $T > 298$ K were calculated by using an average linear thermal expansion coefficient (α) of $9 \times 10^{-6} \text{ K}^{-1}$. This is crude because α depends on Q .

Glassy slags: Molar volumes (V_T) are calculated in an identical manner to that for crystalline phases up to T_g . For temperatures above T_g the molar volume at T_{liq} (V^m) for the liquid is calculated by:

$$V_T = V_{T_g} + (T - T_g) \{ (V^m - V_{T_g}) / (T_{liq} - T_g) \} \quad (56)$$

Most estimated liquid densities lie within $\pm 2\%$ but values obtained for slags containing constituents for which the parameters (used in the calculation) are not been well-defined could be subject to higher uncertainties.

5.4 Surface tension worksheet

No data should be inputted into this worksheet

Surface tension values are calculated (Method 1) using the partial molar method [86] outlined above in Section 4.7.3 and Equn 45 and Figure 25.

$$\gamma = \sum X_i \gamma_i + X_2 \gamma_2 + X_3 \gamma_3 + \dots \quad (45)$$

- The calculated surface tensions using an average $d\gamma/dT = -0.15$ will appear in cells M4 to M9 and are denoted as “a” *ie.* Method1a or 2a
- Values calculated using a $d\gamma/dT$ obtained by $d\gamma/dT = \sum X_i (d\gamma/dT)_i + X_2 (d\gamma/dT)_2 + \dots$ are given in cell O24 and the surface tension values calculated with this γ/dT are given in cells N4 to N9 (note I have been unable to establish $d\gamma/dT$ for some components) These values are denoted b *ie.* Method1b or 2b.

The uncertainty in the estimated values is ca. $\pm 10\%$ the model tends to underestimate the surface tension when the slag contains more than one surfactant *t eg,* B_2O_3 . This is because there will be competition for surface sites between the various surfactants.

Consequently, Method 2 was devised to address this problem. It was assumed that (i) surfactants to occupy the surface would be in the hierarchy of lowest surface tension $B_2O_3 > K_2O > Na_2O > CaF_2 > Fe_2O_3 > Cr_2O_3$ and (ii) that surface saturation occurred at $N=0.12$. The contributions were calculated from the various oxides until $N=0.12$ was attained. Above $N=0.12$ all contributions were taken as positive contributions, $X_i \gamma_i$, for the remaining surfactants *ie.* they were not present in the surface layer and thus contributed normally in the bulk. The values from this method are preferred.

5.6 Viscosity Worksheet

No data should be inputted into this worksheet. The viscosity worksheet contains several models. The chemical composition and T^{liq} are shown on this sheet –**do not insert values here Always ensure these values are changed on the Composition worksheet or the calculations will get corrupted.**

The T^{liq} value inserted on the composition worksheet will appear on Viscosity- cell D19 and temperatures of interest will appear automatically in cells D20- D25 and cells D3 to D8; L38 to R38 and T39 to T45.

5.6.1 Procedures

1. Insert (i) slag composition (cells B4 to B23) and (ii) T_{liq} (cell B28) in Composition worksheet
2. T_{liq} will appear in cell D19 and insert other temperatures of interest in cells **D20 to D25**
3. These temperatures will appear automatically in cells (D3 to D8-Riboud) (J19 to J25- Opt. Bas) and (L38- R38 and T39- T45 for Iida model) –do not insert temperatures into any cells but **D20 to D25 as it may corrupt the software.**
4. Calculated viscosity values will appear in the following cells:
 - Riboud model G3 to G8 and H3 to H8
 - Optical basicity model: K19-K25 and L19 to L25

-MLL model E19 to E25 and F19 to F25

-Iida model Y39-Y45 and Z 39-Y45 and (Forsbacka a, b, c values) AB 39-AB 45 and AC 39-AC 45

Note: the values for units Pas and dPas do not always appear in the same order

5.6.1 Riboud model

This model is simple and is applicable to a wide range of slags. The model divides the slag constituents into 5 different categories; additional slag constituents are covered here and these have been allocated to the various groups and are denoted by {}. The model applies to the following ranges: SiO₂ (28-48%) CaO (13-52%) Al₂O₃ (0-17%) CaF₂ (0-21%) Na₂O (0-27%)

$$X_{\text{SiO}_2} = X_{\text{SiO}_2} + X_{\text{P}_2\text{O}_5} + X_{\text{TiO}_2} + X_{\text{ZrO}_2}$$

$$X_{\text{CaO}} = X_{\text{CaO}} + X_{\text{MgO}} + X_{\text{FeO}} + X_{\text{Fe}_2\text{O}_3} + \{ X_{\text{MnO}} + X_{\text{NiO}} + X_{\text{CrO}} + X_{\text{ZnO}} + X_{\text{Cr}_2\text{O}_3} \}$$

$$X_{\text{Al}_2\text{O}_3} = X_{\text{Al}_2\text{O}_3} + \{ X_{\text{B}_2\text{O}_3} \}$$

$$X_{\text{CaF}_2}$$

$$X_{\text{Na}_2\text{O}} = X_{\text{Na}_2\text{O}} + X_{\text{K}_2\text{O}} + \{ X_{\text{Li}_2\text{O}} \}$$

The temperature dependence is expressed using the Weymann equation:

$$\eta(\text{dPas}) = A T \exp (B/T)$$

$$A = \exp (-19.81 + 1.73 X_{\text{CaO}} + 5.82 X_{\text{CaF}_2} + 7.02 X_{\text{Na}_2\text{O}} - 35.76 X_{\text{Al}_2\text{O}_3}) \quad (57)$$

$$B = 31140 - 23896 X_{\text{CaO}} - 46356 X_{\text{CaF}_2} - 39159 X_{\text{Na}_2\text{O}} + 68833 X_{\text{Al}_2\text{O}_3} \quad (58)$$

5.6.2 Optical basicity (A) model

Mills and Sridhar [83] reported a simple model using the optical basicity (Λ) to represent both the structure and cationic effects, which was applicable to a wide range of slags. The optical basicity was corrected (Λ_{corr}) for charge balancing necessary for Al₂O₃ going into the silicate network; this was done by deducting $X_{\text{Al}_2\text{O}_3}$ from the mole fraction of the network breaker (X_{NB}) with the largest Λ value. Here the deduction was made from X_{NB} for all cations (*ie* assumes the charge balancing is equally shared by all cations). Values used for the various constituents are given in Table 5. Note for CaF₂ n is taken as 1.

Table 5: Optical basicity values used in calculation a value of $\Lambda = 0.61$ was assumed for ZrO₂.

K ₂ O	Na ₂ O	BaO	SrO	Li ₂ O	CaO	MgO	Al ₂ O ₃	TiO ₂	SiO ₂	B ₂ O ₃	Fe ₂ O ₃	Cr ₂ O ₃	FeO	NiO	MnO	CrO	CaF ₂
1.4	1.15	1.15	1.1	1.0	1.0	0.78	0.60	0.61	0.48	0.42	0.75	0.75	1.0	1.0	1.9	1.0	1.2

$$\Lambda = \frac{\sum X_i n_i \Lambda_i}{\sum X_i n_i} \quad (59)$$

Where i= slag constituent eg. CaO ;n= number of O eg 3 for Al₂O₃.

After correction of Λ the viscosity was calculated via Eqns 60-62

$$\ln (B/1000) = -1.77 + 2.88 / \Lambda_{\text{corr}} \quad (60)$$

$$\ln A = -232.69 (\Lambda_{\text{corr}})^2 + 357.32 \Lambda_{\text{corr}} - 144.17 \quad (61)$$

$$\eta(\text{Pas}) = A \cdot \exp (B/T) \quad (62)$$

This model was found not to perform very well and the calculated values do not appear on the Collected worksheet

5.6.3 Iida model

The model [79,80] is based on using the basicity index (B_i) to represent structure:

$$\eta(\text{Pas}) = A \eta_0 \exp (E/B_i) \quad (63)$$

where A =pre-exponential term, E=activation energy; η_0 =hypothetical viscosity for each slag constituent (*i*) ; the parameters A, E and η_0 are all given as functions of temperature.

$$A = 1.029 - 2.078 \times 10^{-3} T + 1.05 \times 10^{-6} T^2 \quad (64)$$

$$E = 28.46 - 2.884 \times 10^{-2} T + 4.0 \times 10^{-6} T^2 \quad (65)$$

$$\eta_0 = \sum \eta_0 X_{\text{SiO}_2} + \eta_0 X_{\text{CaO}} + \eta_0 X_{\text{Al}_2\text{O}_3} + \eta_0 X_{\text{MgO}} + \dots \quad (66)$$

$$\eta_0 = 1.8 \times 10^{-7} \left\{ (M_i T_i^m)^{0.5} \exp(H_i / R^* T) \right\} / \left\{ V_m \right\}_i^{0.6667} \exp(H_i / RT) \quad (67)$$

where V^m = molar volume for each constituent and $H_i = 5.1 (T^m)_i$ and R^* = Gas constant

The various constituents are divided into (1) **acidic** (SiO_2 , ZrO_2 , TiO_2) denoted by A (2) **basic** (CaO , MgO , Na_2O , K_2O , Li_2O , FeO , MnO , CrO , CaF_2 etc denoted B and (3) amphoteric Al_2O_3 , B_2O_3 , Fe_2O_3 , Cr_2O_3 . The basicity index B_i is calculated by

$$B_i = \frac{\sum (\alpha_i \cdot \%i)_B}{\sum (\alpha_i \cdot \%i)_A} \quad (68)$$

where α_i = constant for each constituent expressing its relative basicity and $\%i$ = mass %.

This was the original Iida model. Subsequently, he modified [79,80] it to account for the amphoteric where their basicity changed according to the temperature. This was done through the modified basicity index (B_i^j) particularly for Al_2O_3 which was done through back-calculation from experimental viscosity data (Eqn). It was concluded that Fe_2O_3 and Cr_2O_3 worked basically as basic oxides so they appear on the top line. The model gets exceedingly complicated because the modified α (denoted α^*) for Al_2O_3 was obtained from experimental viscosity data for certain systems eg $\text{CaO} + \text{MgO} + \text{Al}_2\text{O}_3 + \text{SiO}_2$ and then expressed by:

$$(B_i^j) = \left\{ \sum (\alpha_i \cdot \%i)_B + (\alpha_i \cdot \%i)_{\text{Fe}_2\text{O}_3} + (\alpha_i \cdot \%i)_{\text{Cr}_2\text{O}_3} \right\} / \left\{ \sum (\alpha_i \cdot \%i)_A + \sum (\alpha_i \cdot \%i)_{\text{Al}_2\text{O}_3} \right\} \quad (69)$$

$$\alpha_i \cdot \%i = a B_i + b \%_{\text{Al}_2\text{O}_3} + c \quad (70)$$

The model becomes extremely complicated and confusing to predict unknown viscosities because $\alpha_i \cdot \%i$ values are determined for each system/family and there is no general overall value for $\alpha_i \cdot \%i$ eg one can calculate it from a, b and c values for $\text{CaO} + \text{MgO} + \text{Al}_2\text{O}_3 + \text{SiO}_2$ but other a, b, c values (leading to a different $\alpha_i \cdot \%i_{\text{Al}_2\text{O}_3}$) are given for $\text{Li}_2\text{O} + \text{Al}_2\text{O}_3 + \text{SiO}_2$. The high accuracy claimed with this model comes from its calibration with experimental data for each family of slags.

Calculated viscosity values are given for the selected temperatures in cells E19-E25 and F19-F25..

Forsbacka [81,82] gives different a, b, c values for the $\text{CaO} + \text{MgO} + \text{Al}_2\text{O}_3 + \text{SiO}_2$ system values calculated with this are given in cells AB 39-AB45 and AC39-AC45. Values due to Forsbacka were used for CrO and Cr_2O_3 .

5.6.4 Urbain model

This model divides the various slag constituents into :

Glass formers $X_G = X_{\text{SiO}_2}$

Network modifiers: $X_M = X_{\text{CaO}} + X_{\text{MgO}} + X_{\text{CaF}_2} + X_{\text{FeO}} + X_{\text{CaO}} + X_{\text{MnO}} + X_{\text{CrO}} + X_{\text{NiO}} + X_{\text{Na}_2\text{O}} + X_{\text{K}_2\text{O}} + X_{\text{Li}_2\text{O}} + 2 X_{\text{TiO}_2} + X_{\text{ZrO}_2}$

Amphoterics: $X_A = X_{\text{Al}_2\text{O}_3} + X_{\text{B}_2\text{O}_3} + X_{\text{Fe}_2\text{O}_3} + X_{\text{Cr}_2\text{O}_3}$

Here it has been assumed that Fe_2O_3 and Cr_2O_3 behave as network breakers than amphoteric so they have been allocated so that the fraction (f) behaving as network modifiers $f = 0.6$.

Urbain works predominantly on a basis of $M_x\text{O}$ so this creates extra ions and it is necessary to normalise X_G , X_M and X_A by dividing by the term $(1 + 0.5 X_{\text{FeO}1.5} + X_{\text{TiO}_2} + X_{\text{ZrO}_2} + X_{\text{CaF}_2})$ to give X_G^* , X_M^* and X_A^*

The model assumes the Weymann relation

$$\eta(\text{dPas}) = A T \exp(B/T) \quad (71)$$

Urbain [95] found that A and B were linked through the equation

$$-\ln A = 0.29B + 11.57 \quad (72)$$

The B value must be calculated via the equations

$$\alpha^* = X_M / (X_M + X_A) \quad (73)$$

$$B_i = a_i + b_i \alpha + c_i \alpha^2 \quad (74)$$

Where subscript i can be 0, 1, 2 or 3 and a, b and c are given constants for each case eg 0, 1, 2, 3

$$B = B_0 + B_1 X_{SiO_2} + B_2 X_{SiO_2}^2 + B_3 X_{SiO_2}^3 \quad (75)$$

Different values for a, b and c are given for 0, 1, 2, 3 to calculate B values for the CaO- Al₂O₃ + SiO₂, MgO- Al₂O₃ + SiO₂, and MnO- Al₂O₃ + SiO₂ systems. Here X^{“MnO”} represents X_{MnO} + X_{FeO} + X_{NiO} + X_{CrO} + 0.6(X_{Fe₂O₃} + X_{Cr₂O₃}) and the global B (B_{global}) is given by

$$B_{global} = (X_{MnO} B_{MnO} + B_{CaO} X_{CaO} + B_{MgO} X_{MgO}) / (X_{MnO} + X_{CaO} + X_{MgO}) \quad (76)$$

The values calculated with this software are in good agreement with the values cited by Urbain [95]

5.6.5 Mills, Lang and Li (MLL) model

A new model for estimating viscosity was prepared for this course. It assumed an Arrhenius relation for the viscosity.

$$\eta(\text{dPas}) = A \exp(B/T) \quad (77)$$

Values for ln A and B were determined for binary and ternary slag systems and values were derived for both -ln A and B which were then plotted against Q^{corr}. The plots revealed a linear correlations between both B and ln A with Q between Q = 0 and 3.5 with small, systematic deviations from the curve for individual cations eg. Li⁺. These deviations were then plotted against X_{MxO} eg X_{Li₂O}. The resulting equations are given by:

$$\ln A = -6.0 - 1.15Q_{slag} + 8.085 X_{Na_2O+K_2O} - 9.67 X_{Na_2O+K_2O}^2 + (15.1X_{Li_2O} - 17.97X_{Li_2O}^2) + 1.14X_{FeO} - 20X_{Cr_2O_3} - 44.2X_{CaF_2} + 220 X_{CaF_2}^2 \quad (78)$$

$$B = -10000 - 4500Q_{slag} - 21000 X_{Na_2O+K_2O} + 18050 X_{Na_2O+K_2O}^2 - 35666X_{Li_2O} + 36000X_{Li_2O}^2 - 6050 X_{FeO} - 17500 X_{CaF_2} \quad (79)$$

However, the model did not perform well and consistently over-estimated the viscosities and so it has not been cited in the “Collected data”. Details of the model are given in Appendix 2. Further work will be carried out to determine the reasons for the poor performance.

5.7 Thermal conductivity worksheet

Liquid slags

Three methods are given for estimating the thermal conductivity of liquid slags. Experimental data [87-93] for thermal conductivity used here were limited to those using line source techniques because other techniques may yield values containing a large contribution from radiation conductivity

5.7.1 Method 1 - relation with viscosity

This uses the relation of thermal conductivity (k) of the liquid at T^{liq} (k^m) with viscosity. Reported line source data for ln k^m [87-93] were correlated with Riboud calculations of ln η^m; the data showed some scatter because of (i) uncertainties in the calculated ln η^m values (ii) experimental uncertainties associated

with $\ln k^m$ and (iii) sensitivities of both η^m and k^m in the region around T_{liq} and the uncertainties in T_{liq} itself. The following relation was obtained.

$$\ln k^m = -2.178 + 0.282 \cdot \ln \eta^m \quad (80)$$

5.7.2 Method 2 - relation to both Q and $\ln \eta^m$

This method is similar to Method 1 in that it uses a relation between $\ln \eta^m$ and $\ln k^m$. The data shown in Figure 32b (derived with the MLL method) can be expressed as an exponential relation.

$$\eta^m = 0.165 \exp(Q / 0.817) \quad (81)$$

Then $\ln k^m$ can be calculated using the equation

$$\ln k^m = -1.8755 - 0.0893 (\ln \eta^m) + 0.0352 (\ln \eta^m)^2 \quad (82)$$

The values of k^m obtained are only valid for the range $Q=2$ to 3.2 . Care should be taken particularly for slags with $Q > 3.2$ and for slags with high Al_2O_3 contents (eg $45\% CaO + 10\% SiO_2 + 45\% Al_2O_3$ which would show a high Q value but in actual fact, is largely made up of calcium aluminates and will relatively low $\ln \eta^m$; and k^m values).

5.7.3 Method 3 - relation with Q

The relation between $\ln k^m$ and Q is shown in Figure 32a and it can be seen that it has similarities to the equation between $\ln \eta^m$ and Q (Figure 32b, Equn). There is significant dispersion in the scattered data for k^m but the upward trend with increasing Q is obvious. Unfortunately, the experimental values for k^m lie within the range $Q=2$ to 3.2 . The following relation was derived:

$$\ln k^m = -1.914 + 0.00037 \exp(Q/0.402) \quad (83)$$

This equation should not be used out of range ie $Q > 3.2$ or $Q < 2$

The temperature dependence would be expected to follow an Arrhenius –type relation because of the correlation between η and k .

$$\ln k_T (liq) = A \exp(B/T) \quad (84)$$

There are insufficient data to determine B values as a function of Q , so an approximate relation for dk/dT was obtained.

$$dk/dT = 0.0005 \exp(0.5551Q) \quad (85)$$

but should be used with caution.

Solid slags

The experimental data for $\ln k_{298}$ and $\ln k_{Tg}$ show appreciable scatter when plotted vs Q (Figure 33) but they do show k increasing with increasing Q . The data were assumed to follow an exponential relation like that for $\ln k^m$ (Equn 83, Figure 32a). It was noted that the experimental data for solid, Li_2O -containing slags were significantly higher than the curve values and so the correction for Li_2O was added to the exponential relation:

$$\ln k_{298} = -0.424 + 0.00002 \exp(Q / 0.299) + 3.2 \cdot X_{Li_2O} \quad (86)$$

$$\ln k_{Tg} = -0.435 + 0.00005 \exp(Q / 0.332) + 3.0 \cdot X_{Li_2O} \quad (87)$$

This equation should not be used out of range ie $Q > 3.3$ or $Q < 2$

Values can be calculated at other temperatures by linear interpolation between 298 K and T_g and values have also been calculated in the same manner for T_g to T_{liq} (but this should in fact follow a Vogel-Fulcher relation, Eqn 37 but there were too few data to establish the necessary constants). ***This procedure should only be accepted for slags in the range $Q=2$ to 3.3 .***

A second method is also shown. I have found that for slags with Q around 2.5 the thermal diffusivity between 298 K and T_g tend to have a constant thermal diffusivity $a = 4 \times 10^{-7} \text{ m}^2\text{s}^{-1}$; values calculated from $k = a \cdot C_p \cdot \rho$ using the calculated values of C_p and ρ are also shown. These values only apply to $Q=2$ to 3.

Crystalline slags

Nishioka et al. [94] report k values for crystalline slags are between 1.5 and 2.5 times higher than that for the glassy slag and are remain independent of temperature (Figure 31). Thus it has been assumed that $k_{cryst} = 2k_{glass}$ and is independent of temperature from 298 to 1000K

5.8 Electrical conductivity worksheet

The electrical conductivities have been estimated using recent papers by Zhang and Chou [58, 59] both of which involve using the relation between conductivity and viscosity.

5.8.1 Method 1

Chou and Zhang [58, 59] proposed a relation for slags containing CaO, MgO, Al_2O_3 and SiO_2 .

$$\ln k = (-0.08 - \ln \eta) / 1.18 \quad (88)$$

Zhang calculated values of $\ln k$ using this equation and parameters to calculate the viscosity. These are not generally available so $\ln \eta$ values were calculated using the Riboud, Iida and Urbain models.

5.8.2 Method 2

Zhang et al reported that the following equations for M_2O - SiO_2 (where $M_2O = Na_2O$ etc) and MO - SiO_2 (eg CaO) systems (Figure 21)

$$M_2O - SiO_2: \quad \ln k = (.02 - \ln \eta) / 2.87 \quad (89)$$

$$MO - SiO_2 \quad \ln k = (0.15 - \ln \eta) / 1.1 \quad (90)$$

This was attributed to the fact that there are twice as many Na^+ ions as Ca^{2+} for equivalent compositions. The model calculates the ratio of $2 \sum X_{M^+} / \sum (2 X_{M^+} + X_{M_2^+} + 0.667 X_{M_3^+} + 0.5 X_{M_4^+})$ and adjusts Eqn for X_{M^+} ions present in the slag. ***This method should be used when the slag contains M^+ ions eg. Na^+ , K^+ or Li^+ .***

References

1. PV Riboud, and LD Lucas, "Influence of mass transfer upon surface phenomena in iron- and steelmaking", Canadian Metallurgical. Quart. 20: (1981): 199/208.
2. KC Mills: Fundamentals of Metallurgy, edited S Seetharaman, publ. Abington UK (200)
3. K Mukai: Interfacial phenomena in Materials processing edit ED Hondros, M McLean and KC Mills, Book 692 Royal Society, publ IOM, London (1998) p201.
4. AA Kazakov, Y Matveev, L Arykova, L and V Ryabov Russian Metallurgy, (1993) (4) 94-96 see also AA Kazakov, Russian Metallurgy 1997(6): 25-29.
5. S Riaz and KC Mills – REF?
6. DW Bruce and NS Hunter: Proc. 2nd Europ. Conf. on Continuous Casting. Dusseldorf, (1994) 156/161
7. KC Mills, Y Su, AB Fox, Z Li, RP Thackray and H Tsai: A review of slag splashing. ISI J Intl. 45 (2005) 619/633.
8. S Oxley, PN Quedsted and KC Mills: The benefits of using experimental thermophysical property data on defect predictions Proc. AVS Conf. held Santa Fe, NM, Feb. (1999)

9. BO Mysen: Structure and Properties of silicate melts, publ Elsevier, Amsterdam,(1988)
10. BO Mysen: Earth Science Reviews, 27 (1990) 281/365.
11. ME Fleet:X-ray diffraction and spectroscopic studies on the structure of silicate glasses, in short course on silicate melts edit. CM Scarfe, Mineralogical Soc. Ottawa, Canada, Oct (1986)1/35.
12. KC Mills: ISIJ Intl. 33(1993) 148/156.
13. A Shankah:"Studies of high-alumina blast furnace slags""PhD Thesis KTH Stockholm (2007)
14. Du Sichen, J Bygden and S Seetharaman: Metall. Trans. B 25B (1994) 519/525 and 589/595
15. T Tanaka, M Nakamoto and J Lee: Proc. Metal Separation Technology held Copper Mountain, Junre (2004) edited R E Aune andM Kekkonen publ. Helsinki Univ. Technol. 135/142
16. PJ Bray, RV Mulkern and EJ Holupka: J Non-Cryst. Solids 75 (1988) 29/36 and 37/44
17. Jiang Zhongtang and Tang Yongxing: J Non-Cryst. Solids 146 (1992) 57/62.
18. Y Waseda and JM Toguri: The structure and properties of oxide melts, publ. World Scientific, Singapore,(1998)
19. Y Sasaki , M Iguchi and M Hino ISIJ Intl 47 (2007) 346/347 and 638/642 and 1370/1371.
20. T Asada, Y Yamada and K Ito: ISIJ Intl. 48(2008) 120/122.
21. S Sridhar and KC Mills: Ironmaking and Steelmaking 27 (2000) 238/242.
22. M Nakamoto L Forsbacka and L Holappa; Proc. 11th Intl Conf on Ferrochrome processINFACON XI held South Africa, 2007.see also Nakamoto et al ISIJ 47 (2007) 1409/1415
23. M Hanao, M Kawamoto, T Tanaka and M Nakamoto : ISIJ Intl. 46 (2006) 427/433.
24. PV Riboud, Y Roux, LD Lucas and H Gaye: Fachber. Huttenprax. Metallweiterverarb. 19 (1981) 859/869.
25. MTDATA web site: www.npl.co.uk/mtdata/
26. Factsage web site; www.factsage.com/
27. Thermocalc web site; www.thermocalc.com
28. P Taskinen, J Gisby, J Pihlasalo and T Kolhinen: Validation of a new viscosity database with industrial smelting slags, Proc. EMC2009 Int. Conference, Innsbruck (Austria), June(2009,) .
29. Ling Zhang, S Sun and S Jahanshai: Metall Trans B 29B (1998) 177/186
30. Ling Zhang, S Sun and S Jahanshai: Metall Trans B 29B (1998) 187/195.
31. H Gaye and J Welfinger 2nd Intl. Symp. Metall. Slags and glasses edited HA Fine and DR Gaskell publ TMS-AIME Warrendale, PA (1984) 357/275
32. Du Sichen, J Bygden and S Seetharaman: Metall. Trans. B 25B (1994) 519/525 and 589/595
33. M Hayashi and S Seetharaman: CAMP- ISIJ 16 (2003) 860/863
35. L Zhang, S Sun and S Jahanshi: J Non-Cryst Solids 282(2001) 24/29
36. H Ogawa, Y Shiraishi, K Kawamura and T Yokokawa: J Non-Cryst Solids 119 (1990) 151/158
37. KC Mills Fundamentals
- 38a. KD Maglic, A Cezairliyan and VE Peletsky, Compendium of Thermophysical Property Measurement Methods Vol 1 Survey of measurement methods: Vol 2 Recommended Measurement techniques and practices publ. Plenum Press, New York (1984).
- 38b. JO'M Bochriss, JL White and JD MacKenzie: Physico-chemical measurements at high temperatures, publ. London (1959).and
- 38c. R Rapp : Physico- chemical measurements in metals research.,publ. Interscience,New York (1970).
39. C Orlling et al. Iron and Steelmaker (2000) 53/53
40. J Robinson, AT Dinsdale, LA Chapman,PN Quested, BJ Monaghan, JA Gisby and KC Mills: Proc. 2nd Intl. Conf. of Science and Technology of Steelmaking held Swansea, April 2001 publ. IOM, London, 149/160.
41. M Persson, T Matsushita, J Zhang and S Seetharaman: Steel Res Intl. 78 (2007) 102/108
42. KC Mills and BJ Keene: Intl. Materials Review: 32 (1987) 1/120
43. Slag Atlas, publ VDEh , Dusseldorf (1995).
44. Y Bottinga and DF Weill:Amer. J Sci 272 (1972) 438. also Geochim. Cosmochim.Acta 46(1982) 909.
45. Hayashi M Hayashi and S Seetharaman: CAMP- ISIJ 16 (2003) 860/863
46. AI Priven: Sov. J Glass Phys. Chem. 14 (1988) 321
47. G Urbain : Steel Res 58 (1987) 11/116 see also Trans. J Brit. Ceram. Soc. 80 (1981) 139/141.
48. T Iida, H Sakai, Y Kita and K Murakami: High Temp. Mater. Processes, 19 (2000) 153/164.

49. CL Senior and S Srinivasachar: *Energy and Fuels* , 9 (1995)277/283
50. KC Mills and S Sridhar: *Ironmaking and Steelmaking* 26 (1999) 262/268.
51. VK Gupta, SP Sinha and B Raj: *Steel India* 21 (1998) 22/29 see also *Steel India* 17 (1994) 74/ 78.
52. K Koyama: *Nippon Steel Tech. Report*, 34 (1987) 41.
53. JW Kim, J Choi, OD Kwon, IR Lee, YK Shin and JS Park: *Proc. 4th Intl Conf on Molten Slags and Fluxes*, held Sendai (1992) publ. ISIJ, Tokyo 468/473.
54. TA Utigard and A Warczok: *Proc. Copper 95 Intl. Conf.*(1995) vol 4 ,publ. Metall. Soc of CIM 423/437.
55. RG Reddy, JY Yen and Z Zhang: *Proc. 5th Intl. Conf. Molten Slags, Fluxes and Salts: held Sydney* (1997) publ. ISS, Warrendale, PA 203/213 see also *High Temp. Sci* 20 (1990) 195/ 202
56. T Tanaka, M Nakamoto, J Lee and T Usui: *Sci Tech Innovative Ironmaking ,Aiming Energy Half Consumption* held Tokyo Nov. 2003 161/164 se also *CAMP-ISIJ* 16 (2003) 864/ 867.
57. A Kondratiev and E Jak: *Metall. Trans. B* 32B (2001) 1015/1025.
58. GH Zhang KC Chou *Metall. Mater. Trans* 41B (2010) 131/136.
59. GH Zhang, BJ Yan, KC Chou and FS Li: *Relation between viscosity and electrical conductivity of silicate me;ts. Metall. Mater. Trans B* (2011)
60. T Tanaka and T Iida: *Steel Research* 1 (1994) 21/28 .
61. T Tanaka, M Nakamoto and J Lee: *Proc. Metal Separation Technology* held Copper Mountain, Junre (2004) edited R E Aune and M Kekkonen publ. Helsinki Univ. Technol. 135/142.
62. Iida and RIL Guthrie: *The physical properties of liquid metals*, publ. Oxford Science publ. (1988)
63. KC Mills and BJ Keene: *Intl. Materials Review: 32* (1987) 1/120
64. LP Moisou and BP Burluyev *Svar. Proizvodsto*, (1997) (June) 18/20.
65. J Zhang, S Shu and S Wei: *Proc.of the 6th Intl. Conf. Molten Slags, Fluxes and Salts* held Stockholm June (2000).
66. AW Cramb and Jimbo : *Steel Research*, 60 (1989) 157/165
67. ZY Qiao, LT Kang, ZM Cao and BY Yuan: *CAMP- ISIJ* 16 (2003) 868/871.
68. M Hayashi, H Ishii, M Susa, H Fukuyama and K Nagata: *Phys. Chem Glasses* 42 (2001) 6
69. K Nagata and KS Goto: *2nd Intl. Symp.Metallurgical slags and fluxes* edited HA Fine and D Gaskell held Lake Tahoe, NV publ TMS-AIME Warendale, PA (1984) 875/889.
70. S Ozawa and M Susa : *Ironmaking and Steelmakng* 32 (2005) 487/493.
71. M Susa, M atanabe, S Ozawa and R Endo: *Ironmaking and Steelmakng* 34 (2007) 124/130.
72. Y Kang and K Morita: *ISIJ Intl* 46 (2006) 420/426.
73. Y Kang and K Morita private communication 2003
74. M Susa, K Kubota, M Hayashi and KC Mills: *Ironmaking and Steelmakng* 28 (2001) 390/395
75. S Ozawa, R Endo and M Susa: *Tetsu-to-Hagane* 93(2007) 8/14.
76. K Nishioko, T Maeda anf M Shimizu: *ISIJ Intl.* 46 (2006) 427/433.
77. R. Gardon: *Proc 2nd Intl Thermal Conductivity Conference* held Ottawa (1962) 167.
78. Nakamoto, TTanaka, L Holappa and L Hamalainen *ISIJ Intl.* 47 (2007) 216; and 38/43 and 1075/1081.
79. T Iida : *Proceedings of Mills Symposium* held London 2002 edited RE Aune and S Sridhar publ NPL, Teddington
80. T Iida: *CAMP-ISIJ* 2002 15(4)
81. L Forsbacka and L Holappa: *Scand. J Metall* 33(2004) 261/268
82. L Forsbacka and L Holappa: *Proc. VII Intl Conf Molten slags,fluxes and salts* held Capetown, publ SAIMM Johannesburg 2004 129/136.
83. KC Mills ands Sridhar: *Ironmaking and Steelmaking* 26 (1999) 262/268.
84. M Nakamoto, A Kiyose, T Tanaka, L Holappa and M Hamalainen: *ISIJ Intl.* 47 (2007) 38/43.
85. M Nakamoto, T Tanaka, L Holappa and M Hamalainen: *ISIJ Intl.* 47 (2007) 211/216
86. KC Mills : *Estimation of physicochemical properties of coal slags. ACS Symposium Series 301 Mineral matter and ash in coal* edited KS Voorres Amer Chem Soc (1986)195/214.
87. S Ozawa, R Endo and M Susa: *Tetsu-to-Hagane* 93(6) (2007) 8/15.
88. S Ozawa and M Susa: *Ironmaking and Steelmaking* 32 (2005) 487/493
89. M Susa, S Kubota, M Hayashi and KC Mills : *Ironmaking and Steelmaking* 28 (2001) 390/395.
90. M Susa, M Watanabe, S Ozawa and R Endo: *Ironmaking and Steelmaking* 34 (2007) 124/130

91. M Hayashi, H Ishii, M Susa, H Fukuyama and K Nagata: Phys Chem Glasses 42 (2001) 6/11
92. K Nagata Proc. 2nd Intl. Conf. On Metallurgical slags and fluxes held Lake Tahoe, NV, USA (1984) p
93. Y Kang and K Morita: ISIJ Intl. 46 (2006) 520/426.
94. K Nishioka, T Maeda and M Shimizu: ISIJ Intl. 46 (2006) 427/433.
95. G Urbain: Steel Research 58(1987) 111/116.
96. Q Jiao and NJ Themelis: Metall. Trans B 19B (1988) 133/140.
97. RJ Hundermark, S Jahanshahi and S Sun: Proc. IMPC held Cape Town South Africa 2003 and RJ Hundermark Masters Thesis, Univ. of Cape Town (2003) cited in ref 98
98. M Barati and KS Coley; Met. Mater. Trans 37B (2006) 41/49
99. S Jahanshahi, S Sun and L Zhang: Proc.10th Intl. Ferroalloy Congress held Feb (2004) publ. SAIMM www.co.za./Journal/v104no9p529.pdf

APPENDIX 1

Methods of determining structure

The various methods of determining structure are summarised in Table 1. For further details the reader should consult other sources [9-12]

Table 1: Methods used to obtain structural information on melts

Method	Measurement	Structural information obtained
Diffraction X-ray, Neutron, Electron	rdf	1. Bond lengths 2. Co-ordination Numbers 3. Inter-tetrahedral angles T-O-T 4. Overall intermediate structure 5. Local O co-ordination around large cations
Spectroscopy Raman, Infra-red Ultra- Violet		1. Bond lengths 2. Bond angles 3. Identification and concentrations of various anionic units
Nuclear Magnetic Resonance (NMR)	Chemical shift	1. Bond lengths 2. Bond angles 3. Identification and concentrations of various anionic units
Mossbauer	Isomer shift Quadrupole splitting	1. Valence state 2. Co-ordination of environment; identification and concentration of Fe ³⁺ with 4- and 6- fold co-ordination. 1. Distortion of O polyhedron 2. Oxidation state Fe ²⁺ or Fe ³⁺ 3. Co-ordination of Fe ³⁺ (4- or 6- fold)
X-ray absorption spectroscopy	EXAFS XANES	1. Bond lengths 2. Bond angles 3. Co-ordination of specific atoms or ions
X-ray emission (ESCA or XPS) ESR spectroscopy	K _α : K _β	1. Co-ordination of specific atoms or ions 2. Changes in valence state
Luminescence spectroscopy		Co-ordination of Mn ²⁺ , Fe ³⁺ , Ti ³⁺ or S (S ²⁻ or SO ₄ ²⁻)
Chromatography		Distribution of chain lengths of different polymeric units
Property measurement	Density, Molar volume	Packing and co-ordination
	Molar refractivity	Concentrations of N ^{0o} , N ⁰⁻ ; N ⁰²⁻
	Viscosity	1. Activation energies related to bond strength 2. Effect of cations on structure.
	Enthalpy of mixing, or solution	1. Measure of bond strength 2. Effect of different cations including structural ordering
	Electrical / Thermal conductivity	1. Indication of amount of ionic and electronic conduction 2. Information on whether fluorides form Si-F bonds
Molecular dynamics (MD)	Calculations	1. Bond strengths 2. T-O-T angles 3. Co-ordination (e.g. Al is 4- fold in Na ₂ O+Al ₂ O ₃ +SiO ₂ slags)
Thermodynamic modelling	Calculations	Concentration of various anionic polymeric units in melt

APPENDIX 2

Details of MLL model

Underlying principles of model

The model is based on the fact that the viscosity is largely controlled by polymeric structure of the liquid slag. It uses the parameter $Q (=4-NBO/T)$ to represent the structure. The temperature dependence for the liquid is expressed by the Arrhenius equation ($\eta(\text{dPas})= A \exp (B/T)$) where T is in K. The terms, $\ln A$ and B are represented as functions of Q and small corrections are made to these relationships between $\ln A$ and Q and B and Q . These equations were derived from experimental viscosity- temperature data for binary and ternary silicates (Figures A2-1 and A2-2). The parameter Q does not differentiate between different cations and their effect on the structure and on the viscosity. Consequently, small corrections to the basic equation are made to account for the effect of individual cation effects on the viscosity (see Table A2-1).

$$\ln A = -6.0 - 1.15Q_{\text{slag}} + 15.1X_{\text{Na}_2\text{O}+\text{K}_2\text{O}} - 18 X_{\text{Na}_2\text{O}+\text{K}_2\text{O}}^2 + (15.1X_{\text{Li}_2\text{O}} - 17.97X_{\text{Li}_2\text{O}}^2) + 1.14X_{\text{FeO}} - 20X_{\text{Cr}_2\text{O}_3} \quad (\text{A1})$$

$$B = -10000 - 4500Q_{\text{slag}} - 35700 X_{\text{Na}_2\text{O}+\text{K}_2\text{O}} + 36000 X_{\text{Na}_2\text{O}+\text{K}_2\text{O}}^2 - 35666X_{\text{Li}_2\text{O}} + 36000X_{\text{Li}_2\text{O}}^2 - 6050 X_{\text{FeO}} \quad (\text{A2})$$

where X_{M^+} = mole fractions of Na_2O , Li_2O and K_2O

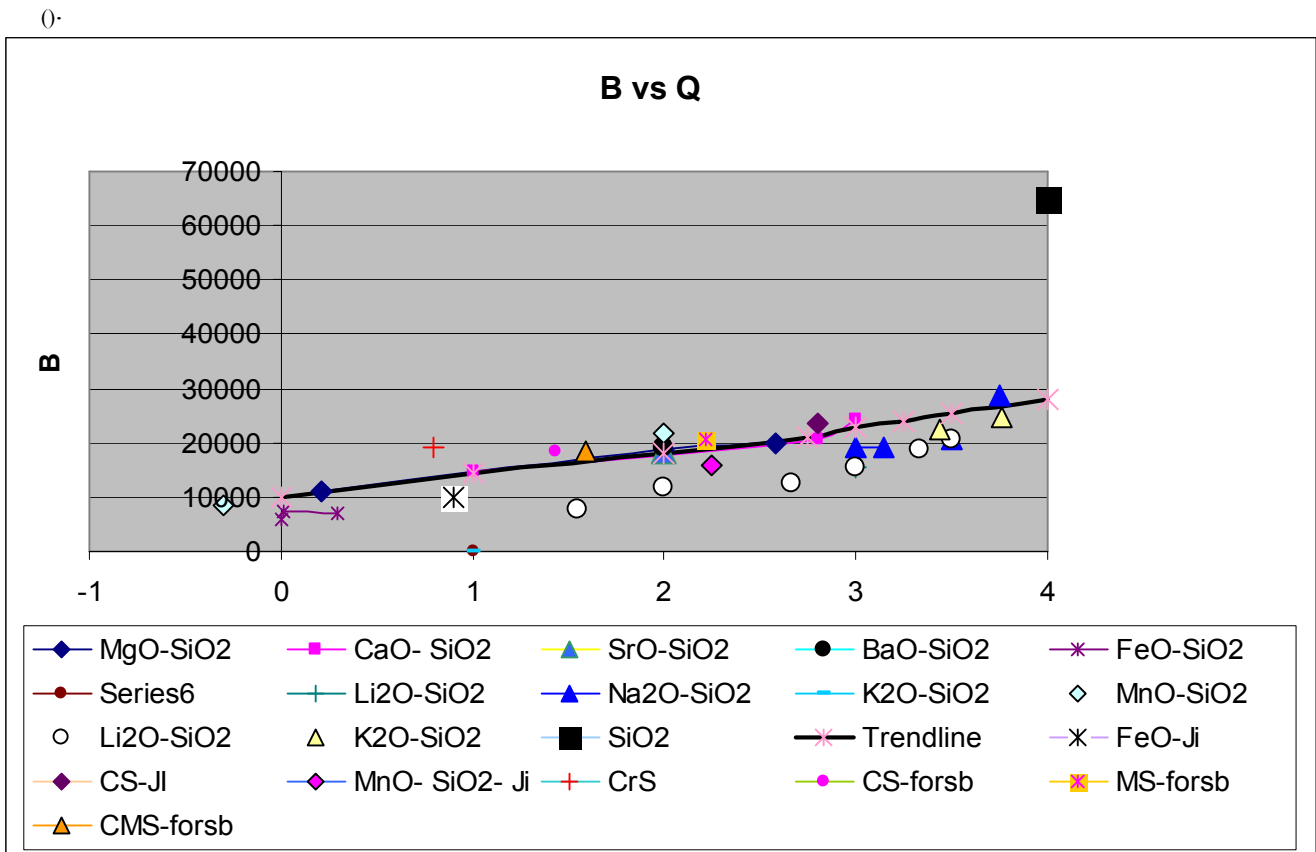


Figure A2.1: The parameter B as a function of Q for binary silicates

The model is valid for silicate slags in the range, $Q=0$ to 4 , (ie. equivalent to range of $2\text{CaO} \cdot \text{SiO}_2$ to SiO_2). Some slags used in metallurgical processes will not be covered eg. some BOS slag compositions and FeO -rich fayalite ($2\text{FeO} \cdot \text{SiO}_2$) slags used in copper production.

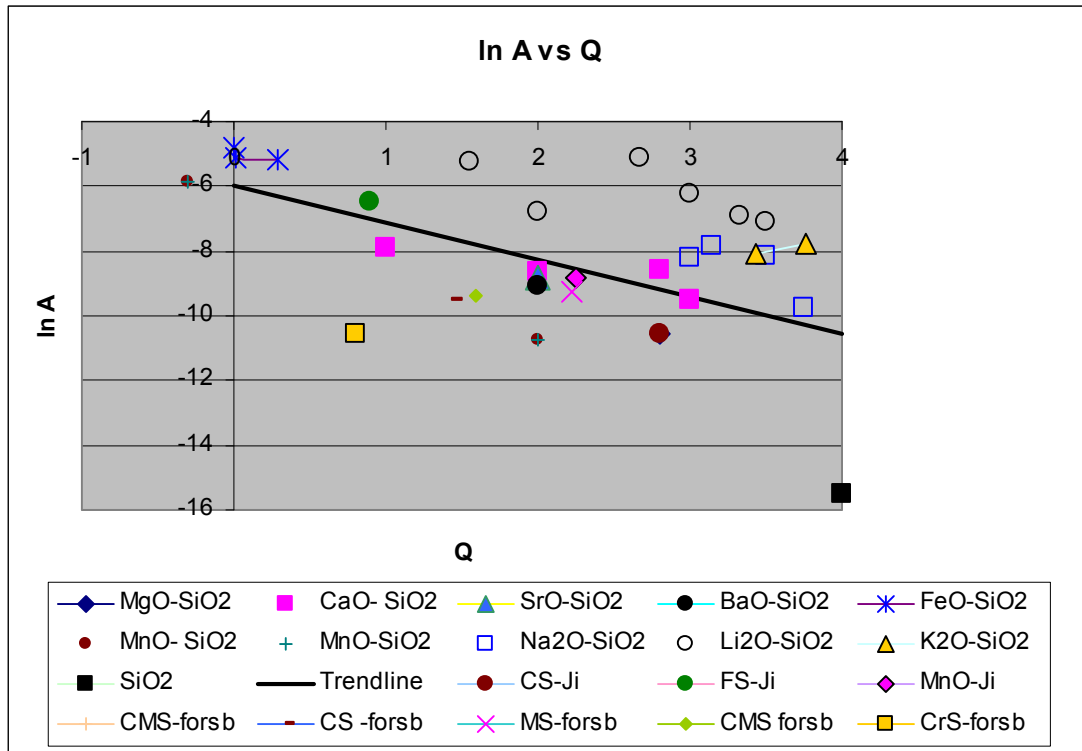


Figure A2.2 The parameter $\ln A$ as a function of Q for binary silicates.

Mould fluxes:

$$\ln A = -6.0 - 1.15Q_{\text{slag}} + 8.085 X_{\text{Na}_2\text{O}+\text{K}_2\text{O}} - 9.67 X_{\text{Na}_2\text{O}+\text{K}_2\text{O}}^2 + (15.1X_{\text{Li}_2\text{O}} - 17.97X_{\text{Li}_2\text{O}}^2) + 1.14X_{\text{FeO}} - 20X_{\text{Cr}_2\text{O}_3} - 44.2X_{\text{CaF}_2} + 220 X_{\text{CaF}_2}^2 \quad (\text{A2-3})$$

$$B = -10000 - 4500Q_{\text{slag}} - 21000 X_{\text{Na}_2\text{O}+\text{K}_2\text{O}} + 18050 X_{\text{Na}_2\text{O}+\text{K}_2\text{O}}^2 - 35666X_{\text{Li}_2\text{O}} + 36000X_{\text{Li}_2\text{O}}^2 - 6050 X_{\text{FeO}} - 17500 X_{\text{CaF}_2} \quad (\text{A2-4})$$

Table A2-1: Details of effects of different cations

Constituent	Observation	Cause, Remedy
Na ₂ O, K ₂ O, Li ₂ O	M ⁺ ions do not bond two chains together like Ca ²⁺ - consistent deviations from B and ln A vs Q	Small corrections to equns of lnA and B vs Q involving $X_{M^+} = \sum X_{\text{Na}_2\text{O}} + X_{\text{K}_2\text{O}} + X_{\text{Li}_2\text{O}}$
FeO	Found to give consistent deviations from lnA and B vs Q relations	Small corrections made to lnA and B vs Q equns
Fe ₂ O ₃	Experimental ln A and B values used to determine Q and f. Mean values of f=0.55; f=0.67-0.086Q	Calculates Q using f=0.55 then recalculates Q using f= 0.67 -0.086Q
Cr ₂ O ₃	Experimental B values used to determine Q and f. Mean values of f=0.45; f=0.73-0.113 Q Experimental ln A values consistently more negative can not be used for f	Calculates Q using f=0.45 then recalculates Q using f= 0.73 -0.113Q Correction to ln A value ; -20X _{Cr₂O₃}
B ₂ O ₃	Exhibits mixture of 3- and 4- coordination in borates and boro-silicates. Additions (<5%) to mould fluxes reduce viscosity and T _{liq}	Program not suitable for high concentrations Taken as a network breaker in low concentrations
MnO	Some of B values reported for high-MnO slags [??] show departure from B vsQ relations	No corrections made to relation
TiO ₂ ZrO ₂	TiO ₂ reported to reduce viscosity [??]- acts as network breaker -assumed ZrO ₂ -identical	TiO ₂ and ZrO ₂ taken as network breakers
CaF ₂	F ⁻ reported to bond with Ca ²⁺ -leaving more-polymerised slag	CaF ₂ ignored in calculation of Q- special calculations needed for slags containing F

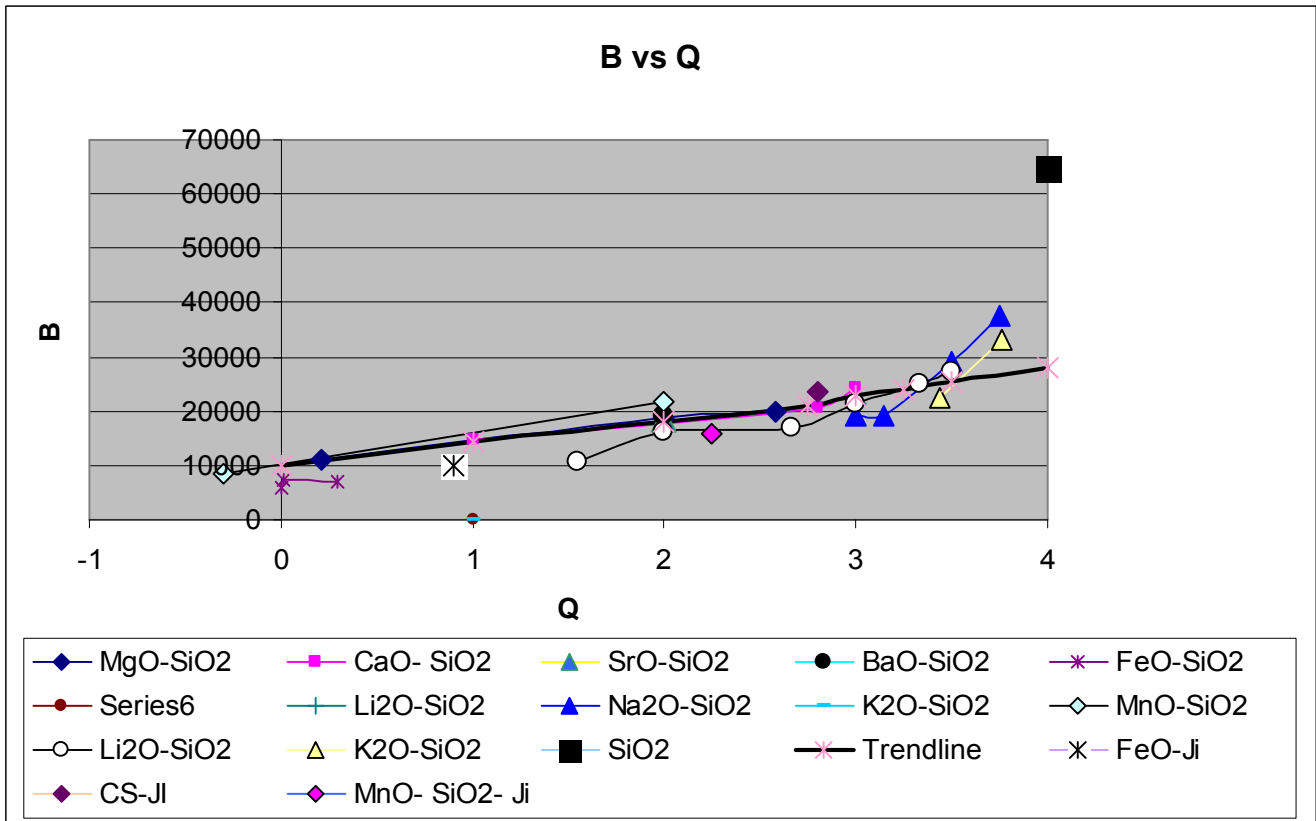


Figure A2-3 Plot of B as a function of Q for binary silicates

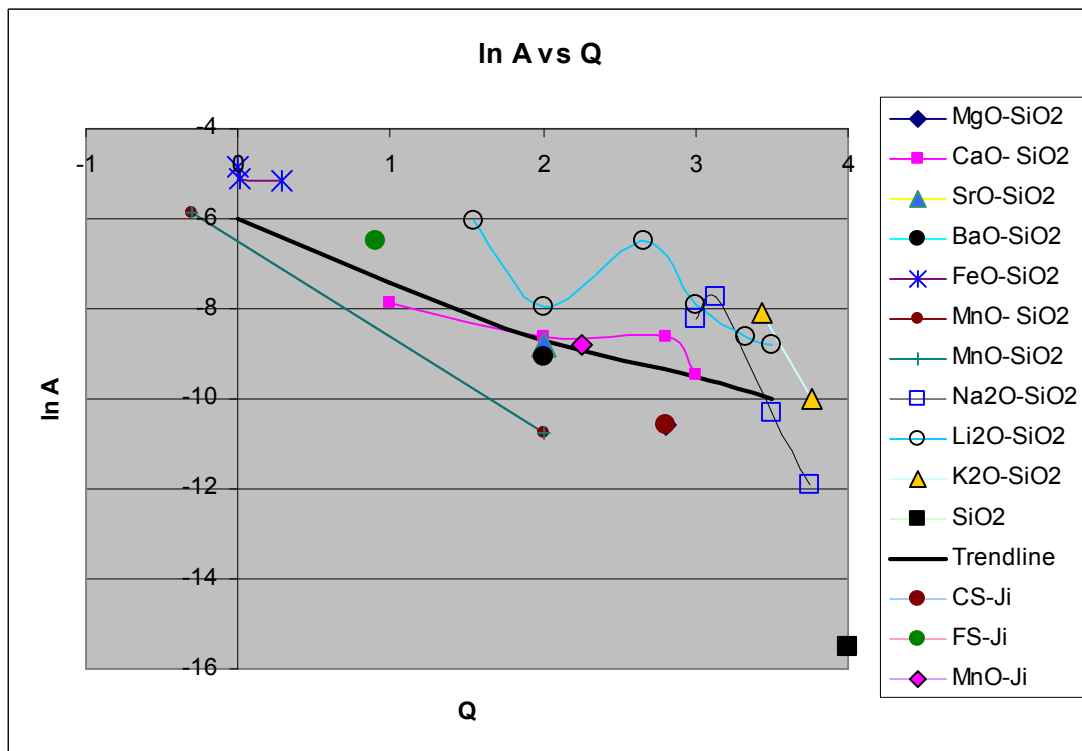


Figure A2-4. Plot of $\ln A$ as a function of Q for binary silicates

There is some dispersion of the data in the range $Q=3.5$ to 4 . It should be noted that $Q=4$ is the equivalent of pure SiO_2 which would cause an upward move to a higher B and a downward move to a more negative $\ln A$ value. However, other slags with compositions where the mole fraction of network breaker exactly charge balances the mole fraction of Al_2O_3 (eg $mX_{\text{CaO}} + mX_{\text{Al}_2\text{O}_3} + (1-2m)X_{\text{SiO}_2}$) also have $Q=4$. These latter cases can be seen as a mixture of SiO_2 and $\text{CaO Al}_2\text{O}_3$ and the deviation from the linearity decreases with increasing “ m ” ie decreasing X_{SiO_2} . It should also be pointed out that these slags with $Q=4$ tend to have high T_{liq} and viscosity measurements are frequently restricted to temperature ranges of $<100\text{K}$ which

leads to lnA and B values with much higher uncertainties. The linear relationship has been adopted for the the range Q=3.5 to 4 but uncertainties in calculated viscosities will be larger than in the range Q =0 to 3.5. The software will calculate Q for the specified composition using Eqns A2.5 to A2.8 where f=fraction of Fe₂O₃ or Cr₂O₃ acting as a network breaker (6-fold coordination).

$$NBO = 2 \{ X_{CaO} + X_{MgO} + X_{Na_2O} + X_{K_2O} + X_{Li_2O} + X_{FeO} + X_{MnO} + X_{CrO} + X_{NiO} + 2X_{TiO_2} + 2X_{ZrO_2} + 3 f_1 X_{Fe_2O_3} + 3 f_2 X_{Cr_2O_3} - X_{Al_2O_3} - X_{B_2O_3} - (1 - f_1) X_{Fe_2O_3} - (1 - f_2) X_{Cr_2O_3} \} \quad (A2-5)$$

$$T' = \{ X_{SiO_2} + 2X_{Al_2O_3} + 2X_{B_2O_3} + 2(1 - f_1) X_{Fe_2O_3} + 2(1 - f_2) X_{Cr_2O_3} \} \quad (A2-6)$$

$$NBO/T = NBO / T' \quad (A2-7)$$

$$Q = 4 - (NBO/T) \quad (A2-8)$$

Use of Model

1. Insert T_{liq} and appropriate temperatures into cell (Composition B28 and Viscosity B19) and cells (Viscosity –B19-B25) respectively.
2. The program will calculate Q (cell B20) ln A (cell) and B and the viscosity (dPAs) (cellB21) and ln viscosity (dPas) (cell B22)